scientific reports

OPEN

Cinnamic acid conjugated with triazole acetamides as anti-Alzheimer and anti-melanogenesis candidates: an in vitro and in silico study

Amir Shervin Shokouhi Asl[1], Mohammad Hosein Sayahi[2], Mohammad Hashem Hashempur[3], Cambyz Irajie[4], Amir Hossein Alaeddini[5], Seyedeh Niloufar Ghafouri[5], Milad Noori[8], Navid Dastyafteh[8], Javad Mottaghipisheh[6], Mehdi Asadi[1], Bagher Larijani[1], Mohammad Mahdavi[8]✉ & Aida Iraji[7]✉

In this study, new cinnamic acid linked to triazole acetamide derivatives was synthesized and evaluated for anti-Alzheimer and anti-melanogenesis activities. The structural elucidation of all analogs was performed using different analytical techniques, including ^{1}H-NMR, ^{13}C-NMR, mass spectrometry, and IR spectroscopy. The synthesized compounds were assessed in vitro for their inhibitory activities against acetylcholinesterase (AChE), butyrylcholinesterase (BChE), and tyrosinase enzymes. Among synthesize derivative compound 3-(4-((1-(2-((2,4-dichlorophenyl)amino)-2-oxoethyl)-1H-1,2,3-triazol-4-yl)methoxy)-3-methoxyphenyl)acrylic acid (10j) exhibited the highest activity against BChE with an IC_{50} value of 11.99 ± 0.53 µM. Derivative 3-(3-methoxy-4-((1-(2-oxo-2-(p-tolylamino)ethyl)-1H-1,2,3-triazol-4-yl)methoxy)phenyl)acrylic acid (10d), bearing a 4-CH_3 group, was identified as the most potent AChE inhibitor. In terms of tyrosinase inhibition, 3-(3-methoxy-4-((1-(2-((2-methyl-4-nitrophenyl)amino)-2-oxoethyl)-1H-1,2,3-triazol-4-yl)methoxy)phenyl)acrylic acid (compound 10n), demonstrated 44.87% inhibition at a concentration of 40 µM. Additionally, a kinetic study of compound 10j which 2,4-dichlorophenyl substituents against BChE revealed a mixed-type inhibition pattern. Furthermore, molecular docking and molecular dynamic studies of compound 10j were conducted to thoroughly evaluate its mode of action within the BChE active site.

Cinnamic acid, chemically known as (E)-3-phenylprop-2-enoic acid, plays a pivotal role in plant biochemistry as an important active ingredient of *Cinnamomum cassia* Presl, and in the biosynthesis of numerous secondary metabolites such as lignans, flavonoids, and stilbenes[1–3]. Cinnamic acid has gained the attention of medicinal chemists and drug designers due to its diverse biological activities. Over time, different cinnamic acid-based derivatives have been developed, exhibiting different pharmacological effects, including antioxidant, anti-inflammatory, antidiabetic, antimicrobial, and anticancer activities[4–8]. The underlying mechanisms behind these effects involve interactions with various cellular targets such as enzymes, receptors, and signaling pathways. By

[1]Department of Medicinal Chemistry, School of Pharmacy, Iran University of Medical Sciences, Tehran, Iran. [2]Department of Chemistry, Payame Noor University, Tehran, Iran. [3]Research Center for Traditional Medicine and History of Medicine, Department of Persian Medicine, School of Medicine, Shiraz University of Medical Sciences, Shiraz, Iran. [4]Department of Medical Biotechnology, School of Advanced Medical Sciences and Technologies, Shiraz University of Medical Sciences, Shiraz, Iran. [5]School of Chemistry, College of Science, University of Tehran, Tehran, Iran. [6]Department of Aquatic Sciences and Assessment, Swedish University of Agricultural Sciences, 7050SE-750 07, Uppsala, Sweden. [7]Stem Cells Technology Research Center, Shiraz University of Medical Sciences, Shiraz, Iran. [8]Endocrinology and Metabolism Research Center, Endocrinology and Metabolism Clinical Sciences Institute, Tehran University of Medical Sciences, Tehran, Iran. ✉email: momahdavi@sina.tums.ac.ir; aida.iraji@gmail.com; iraji@sums.ac.ir

leveraging the adaptability of their structural modifications, cinnamic acid derivatives hold significant potential for developing new treatments that may be more effective and have fewer side effects. These compounds show promise to target Alzheimer's disease (AD) and melanogenesis disorders[9–11].

Melanogenesis, the intricate process of melanin biosynthesis, involves a cascade of enzymatic reactions culminating in the production of eumelanin and pheomelanin. The enzyme tyrosinase plays a key role in melanin synthesis. This copper-containing enzyme is primarily located in melanocytes, the specialized cells responsible for producing melanin[12,13]. Tyrosinase catalyzes the conversion of the amino acid L-tyrosine into L-dopa and subsequently dopaquinone, which serves as a crucial precursor for both eumelanin and pheomelanin synthesis. Dysregulation of tyrosinase activity can lead to various dermatological conditions, including hyperpigmentation, hypopigmentation, and melanoma[14]. In recent years, researchers have focused on identifying natural compounds with tyrosinase-inhibitory properties to address hyperpigmentation disorders and develop novel skin-lightening agents. Cinnamic acid and its derivatives, found abundantly in plants, have emerged as potent tyrosinase inhibitors. Derivatives such as compounds **A–D**, (Fig. 1)[15–18] as potent inhibitors.

AD stands as one of the most pressing global health challenges of the 21st century, characterized by its progression and profound impact on cognitive function. AD is marked by the accumulation of abnormal protein aggregates, including beta-amyloid plaques and tau tangles, in the brain[19]. These pathological changes result in synaptic dysfunction, neuronal loss, and cognitive decline. One of the key neurotransmitter imbalances linked to AD is acetylcholine (ACh), a vital neurotransmitter that plays a major role in memory, learning, and overall cognitive function. Acetylcholinesterase (AChE) and butyrylcholinesterase (BChE) are two critical enzymes responsible for breaking down ACh through hydrolysis. Reduced ACh levels, resulting from the degeneration of cholinergic neurons, lead to cognitive deficits characteristic of AD[20,21]. As a result, cholinesterase inhibitors have emerged as a keystone of AD pharmacotherapy, increasing the level of ACh in the synaptic cleft and junction. Recent research has shown that cinnamic acid derivatives possess the potential to modulate pathways implicated in AD pathogenesis, including the attenuation of neuroinflammation, reduction of oxidative stress, and enhancement of neurotrophic factors. Recent studies have introduced several potent reagents as highly effective cholinesterase inhibitors including thiosemicarbazide[22], quinazolinone[23–25], and sulfonated quinazolinone[26], and thiazolidin-4-one[27]. These findings confirm the importance of cholinesterase as a valid target for managing AD.

Derivatives such as **E**[28], **F**[29], and **G**[30] were introduced as effective ChE inhibitors. The presence of triazole acetamide, widely presented in AChE and BChE inhibitors **H**, **I**, and **J**, provides a suitable moiety to interact
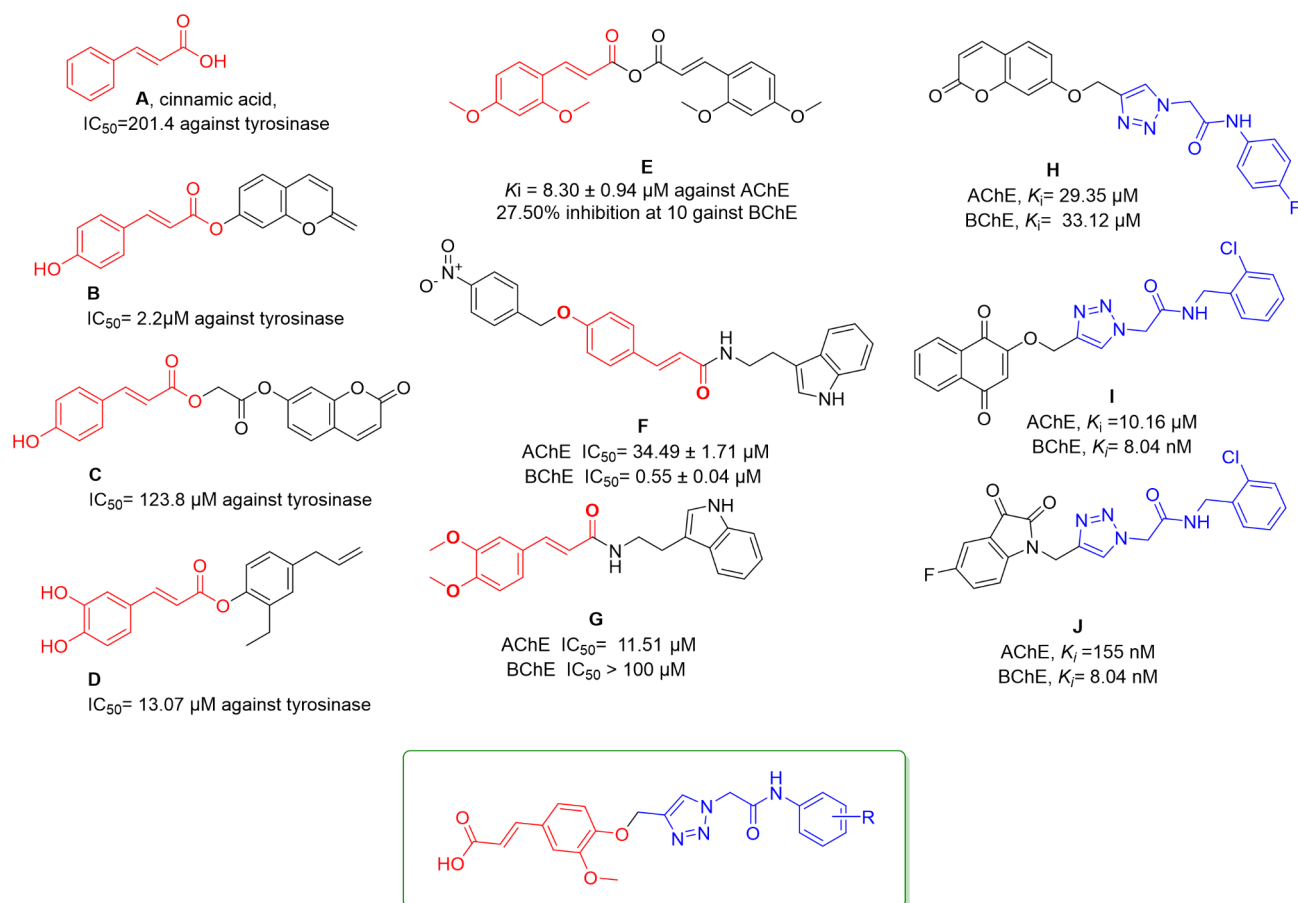

A, cinnamic acid,
IC_{50}=201.4 against tyrosinase

B
IC_{50}= 2.2 µM against tyrosinase

C
IC_{50}= 123.8 µM against tyrosinase

D
IC_{50}= 13.07 µM against tyrosinase

E
Ki = 8.30 ± 0.94 µM against AChE
27.50% inhibition at 10 against BChE

F
AChE IC_{50}= 34.49 ± 1.71 µM
BChE IC_{50}= 0.55 ± 0.04 µM

G
AChE IC_{50}= 11.51 µM
BChE IC_{50} > 100 µM

H
AChE, K_i= 29.35 µM
BChE, K_i= 33.12 µM

I
AChE, K_i =10.16 µM
BChE, K_i= 8.04 nM

J
AChE, K_i =155 nM
BChE, K_i= 8.04 nM

Fig. 1. Designing strategy.

with these enzymes and offers an appropriate site for derivatization to study structure-activity relationships (SAR)[31–34].

There are established links between certain skin disorders and neurodegenerative diseases, including AD and multiple sclerosis. Some risk factors have been reported regarding the neurodegenerative diseases and melanoma. Human tyrosinase, an enzyme involved in the biosynthesis of neuromelanin in the brain and melanin in the skin, as well as AChE and BChE is proposed to play a key role in these connections[35,36]. Hybrids of pharmacophoric moieties have been a key strategy in designing new molecules with enhanced potency. In line with our efforts to discover more potent pharmaceutical agents, hybrids of cinnamic acid as a natural compound, with different triazoles were developed and assessed for their anti-AChE, anti-BChE, and anti-tyrosinase activities. Additionally, kinetic studies and computational evaluations were conducted to further analyze their effects.

Result and discussion
Chemistry
The synthetic procedure for cinnamic acid derivatives conjugated to various triazole acetamide derivatives, **10a-o**, is outlined in Scheme 1. Briefly, 4-hydroxy-3-methoxybenzaldehyde **1** (1 mmol) was added to a solution of K_2CO_3 (1.1 equiv) in DMF and stirred while propargyl bromide **2** (1.1 equiv) was added dropwise at room temperature. Upon completion, the reaction mixture was quenched with water, leading to the precipitation of compound **3**. Subsequently, aniline derivatives **4a–o** (2 mmol) were reacted with chloroacetyl chloride[5] in acetone at room temperature for 30 min to yield N-phenyl-2-chloroacetamides **6a–o**. These intermediates were then converted into azides **7a–o** by reaction with sodium azide and triethylamine (Et$_3$N) in a H_2O/t-BuOH mixture. Compound **3**, in the presence of sodium ascorbate and CuSO₄·5 H₂O (7 mol%), catalyzed the formation of 1,2,3-triazoles **8a–o**. Finally, these triazoles were reacted with malonic acid, piperidine, and pyridine under reflux conditions to afford the final products **10a–n** after purification.

To ensure thorough elucidation, the characterization of compound **10a** was discussed in detail. FT-IR spectrum includes a stretch bond in 3220 cm^{-1} related to NH amide, CH aromatic, and aliphatic are observed in 3030 and 2940 cm^{-1}, respectively. A sharp peak related to C=O is also observed in 1662 cm^{-1}. ^{1}H NMR spectrum of this compound shows the singlet of the acidic proton in 12.20, and the singlet of the amide proton in 10.40. Protons of aromatics are located in 8.25 (s, 1H), 7.41 (s, 1H), 7.36 (d, $J = 8.1$ Hz, 1H), 7.32 (s, 1H), 7.23–7.17 (m, 3 H), and 6.89 (d, $J = 7.5$ Hz, 1H). The olefinic protons are observed in 7.53 (d, $J = 15.9$ Hz, 1H), and 6.45 (d, $J = 16.0$ Hz, 1H). Two singlet peaks related to methylenes are located in 5.33, and 5.19. The singlet peak in 3.79 is related to methoxy and the protons of methyl group are located in 2.26. For the ^{13}C-NMR spectrum, the carbonyl peaks are located at 168.33, and 164.55. The aromatic and olefinic peaks are located in 149.91, 149.60, 144.53, 142.63, 138.78, 138.59, 129.20, 127.93, 126.96, 124.94, 122.90, 120.23, 117.38, 116.87, 113.43, 111.00, and the aliphatic peaks are observed in 61.94, 55.99, 52.68, 21.61.
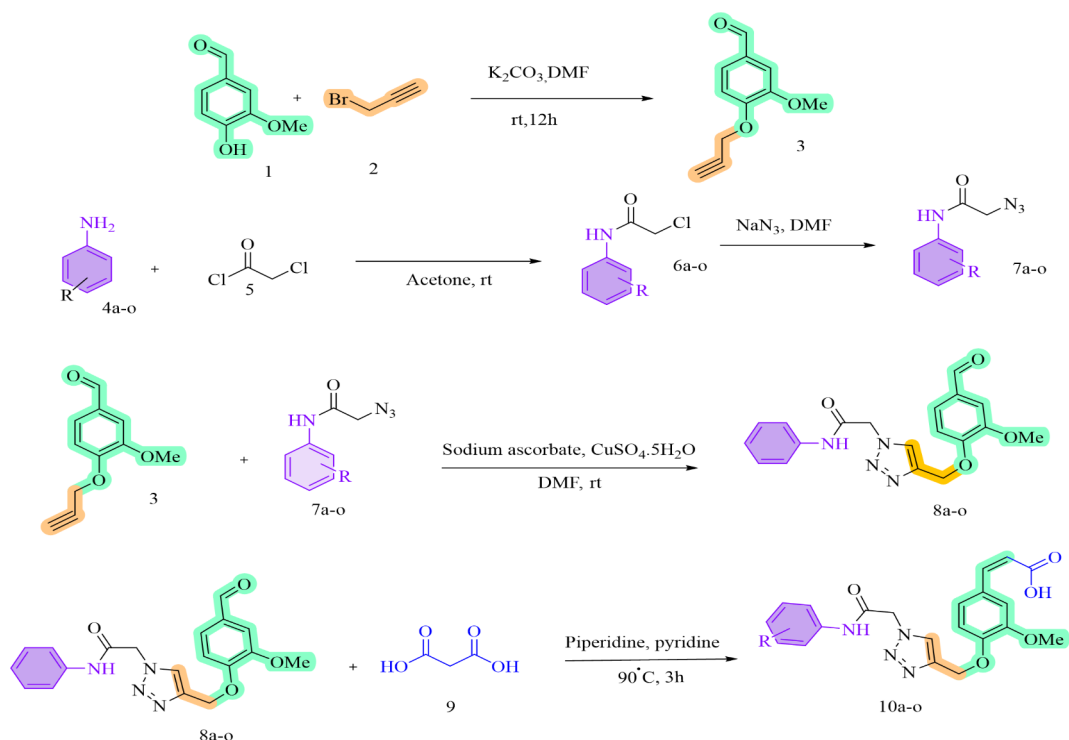
Scheme 1. Synthesis of cinnamic acid derivatives conjugated to various triazole acetamide derivatives, **10a-o**.

Structure-activity relationships against AChE and BChE

The enzyme inhibitory effects of all the newly synthesized compounds (**10a–o**) were first evaluated against AChE and BChE, compared to donepezil. The structure-activity relationships (SAR) and results were deduced as follows (Table 1).
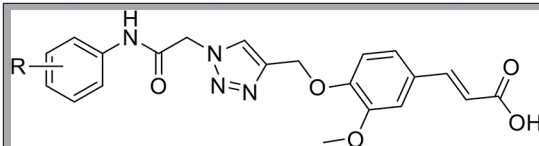
Compound **10a**, an unsubstituted analog, demonstrated weak potency against the AChE enzyme with moderate potency against BChE. Next, methyl, an electron-donating group with a small size, was substituted at different positions of the phenyl ring. In all cases, an improvement in potency was observed *vs.* **10a**. For AChE inhibition, the potency order was 4-methyl (**10d**) > 2-methyl (**10b**) > 3-methyl (**10c**), and for BChE inhibition, the order was the same: 4-methyl (**10d**) > 2-methyl (**10b**) > 3-methyl (**10c**). Given that the 4-methyl substitution was the most potent analog compared to other methyl positions, it was replaced with 4-hydroxy (**10e**), a strong electron-donating group with lower lipophilicity. This resulted in a slight reduction in activity against both enzymes.

In the next round of modifications, compounds **10f-j**, bearing halogen-substituted groups, were synthesized. Compound **10f**, with a 4-fluorine moiety, a small and strong electron-withdrawing group, exhibited weak anti-AChE potency but demonstrated $39.44 \pm 4.99\%$ inhibition against BChE. Among the halogen-substituted groups, the 4-chloro moiety in compound **10i** was the most potent analog against AChE. Notably, the 2,4-dichloro moiety in compound **10j** was categorized as the most active anti-BChE agent, with an IC_{50} value of 11.99 ± 0.53 µM. The high potency of this group might be due to the increased bulkiness of the substituted moiety. As a result, compound **10i**, with 34.79% inhibition, was the most potent anti-AChE agent in halogen derivatives, and compound **10k**, bearing 2,4-dichloro, was categorized as the most active BChE inhibitor among the halogen-substituted groups.

To properly evaluate the effect of electron-withdrawing groups, halogen moieties were replaced with nitro groups, which are polar and strong electron-withdrawing groups. This resulted in decreased potency against BChE in **10k-m**. Compound **10m** exhibited better results against AChE, with 37.56% inhibition at 40 µM. Interestingly, the addition of a 2-methyl group to compound **10m** resulted in compound **10n**, which exhibited better potency against BChE with 32.24% inhibition compared to 25.58% inhibition against AChE, confirming the role of bulky groups in improving BChE inhibition.

Interesting results were observed with the elongation of the linker in compound **10o**. In this case, a reduction in activity was recorded against BChE compared to compound **10a**, while a twofold improvement in potency against AChE was observed compared to compound **10a**. It was proposed that such modification increases the chance of rotation of the molecule in the enzyme binding site.

In summary, for AChE inhibition, the 4-methyl group (**10d**) provides the best inhibition due to optimal steric and electronic effects, followed by 4-nitro, (**10m**) which enhances interactions with the enzyme. The 4-position (*para*) is generally favorable for activity, while the 2-position (*ortho*) of the bulk group is unfavorable due to the intolerance of the spacious group. For BChE inhibition, the 2,4-dichloro substitution is the most active (**10j**), suggesting that increased bulkiness is beneficial for binding.

Entry	R	AChE % inhibition at 40 µM[a]	BChE % inhibition at 40 µM[a]	Tyrosinase % inhibition at 40[b]
10a	H	6.43 ± 0.55	23.96 ± 1.64	10.41 ± 2.851
10b	2-Methyl	30.93 ± 2.11	44.56 ± 4.73	15.98 ± 1.39
10c	3-Methyl	15.99 ± 0.37	18.50 ± 1.42	13.47 ± 3.54
10d	4-Methyl	45.96 ± 1.58	48.48 ± 3.11	13.16 ± 2.19
10e	4-Hydroxy	29.99 ± 1.87	30.35 ± 0.68	10.36 ± 3.48
10f	4-Flurine	9.37 ± 0.98	39.44 ± 4.99	14.19 ± 2.52
10g	2-Chloro	22.30 ± 0.91	20.03 ± 2.18	16.19 ± 1.92
10h	3-Chloro	25.52 ± 1.04	15.35 ± 4.04	11.42 ± 1.80
10i	4-Chloro	34.79 ± 2.23	22.23 ± 1.12	12.34 ± 1.53
10j	2,4-diChloro	26.12 ± 0.20	58.21 ± 2.09	7.73 ± 2.73
10k	2-Nitro	22.09 ± 2.17	25.23 ± 1.94	11.51 ± 2.13
10l	3-Nitro	30.01 ± 3.41	20.51 ± 0.94	12.07 ± 3.84
10m	4-Nitro	37.56 ± 1.06	18.67 ± 2.84	13.97 ± 3.11
10n	2-Methyl-4-nitro	25.58 ± 1.59	32.24 ± 1.98	44.87 ± 6.66
10o	Phenylethyl	18.38 ± 1.20	14.89 ± 0.89	10.37 ± 2.34

Table 1. Biological evaluation of cinnamic acid derivatives conjugated to different triazole acetamides. [a] Data present here are the mean ± S.E and donepezil as positive control exhibited $IC_{50} = 0.079 \pm 0.05$ µM against AChE and $IC_{50} = 10.6 \pm 2.1$ µM against BChE. [b] Kojic acid positive control $IC_{50} = 27.56 \pm 1.27$ µM.

SAR assessments of substituted aryl triazole compounds were discussed here to compare with our findings. A study on naphthoquinone-triazole acetamide derivatives indicated that derivatives with halogen substituents are highly effective AChE and BChE inhibitors. For example, compound **K** (Fig. 2), featuring a 2-chloro substituent, demonstrated impressive inhibition constants (K_i) of 10.16 nM for AChE and 8.04 nM for BChE. In comparison, the positive control, tacrine, exhibited K_i values of 70.61 nM for AChE and 64.18 nM for BChE[32]. In another study, compound **L** bearing methoxy demonstrated strong AChE inhibition with an IC_{50} of 0.458 μM, outperforming galantamine, which had an IC_{50} of 0.568 μM; however, its BChE inhibitory activity was weaker, with an IC_{50} of 1.721 μM[37]. Additionally, among the coumarin–1,2,3-triazole–acetamide hybrids, compound **M**, which is 2-chloro, exhibited significant inhibitory effects against both cholinesterases, with K_i values ranging from 27.17 to 1,104.36 nM for AChE and from 590.42 to 1,104.36 nM for BuChE[31]. Furthermore, a related study indicated that the introduction of fluorine atom in compound **N** (3,4-difluoro derivative) resulted in potent BChE inhibitor, with an IC_{50} of 21.71 μM[38]. Overall, SAR studies consistently suggest that halogenated groups enhance inhibitory activity, supporting our findings. As shown in Fig. 2, the 2,4-dichloro-substituted compound (**10j**) was a potent and selective BChE inhibitor, while the 2-methyl-substituted compound (**10d**) effectively inhibited both AChE and BChE.

Structure-activity relationships against tyrosinase

In this study, compounds (**10a-o**) were synthesized and evaluated for their tyrosinase inhibitory activity to understand the impact of different substituents at the R position. The parent compound (**10a**) exhibited weak tyrosinase inhibition (10.41%). Subsequent modifications aimed to enhance this activity by introducing various substituent.

The introduction of methyl groups at different positions (**10b-d**) resulted in slightly improved potency. *Ortho* methyl substitution (2-methyl) showed the highest inhibition among these compounds. Substitutions with hydroxyl (4-hydroxy) (**10e**) did not show significant improvement in activity compared to the parent compound (**10a**).
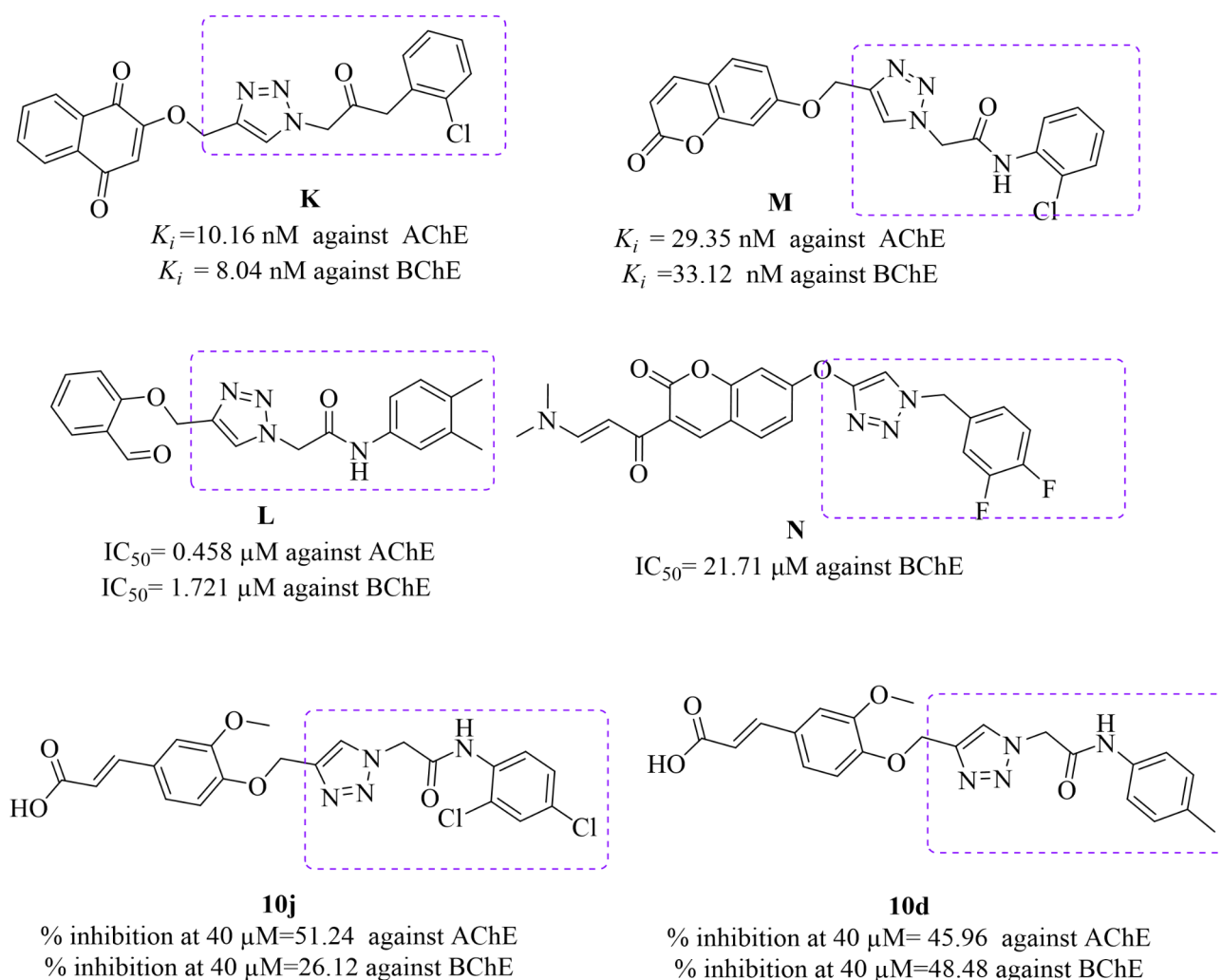

K
K_i =10.16 nM against AChE
K_i = 8.04 nM against BChE

M
K_i = 29.35 nM against AChE
K_i =33.12 nM against BChE

L
IC_{50}= 0.458 μM against AChE
IC_{50}= 1.721 μM against BChE

N
IC_{50}= 21.71 μM against BChE

10j
% inhibition at 40 μM=51.24 against AChE
% inhibition at 40 μM=26.12 against BChE

10d
% inhibition at 40 μM= 45.96 against AChE
% inhibition at 40 μM=48.48 against BChE

Fig. 2. Comparison of SAR from previous studies with findings from the present work against ChE.

Halogen substitutions (**10f-j**) generally enhanced activity compared to compound **10a**. **10f** (4-flurine) showed the best potency among halogen derivatives. Chlorine substitutions exhibited varied effectiveness, with 2-chloro (**10g**) being the most potent in chlorine analogs followed by 4-chloro (**10i**) and 3-chloro (**10h**). The electron-withdrawing nature of halogens enhances the potency against tyrosinase by stabilizing the enzyme-inhibitor complex. However, the reduced activity of 2,4-dichloro (**10j**) suggests that excessive bulkiness and increased lipophilicity can interfere with optimal binding to tyrosinase.

Nitro substitutions (**10k-m**) at various positions did not consistently improve inhibitory activity. Compound (**10n**), bearing 2-methyl-4-nitro, exhibited the highest inhibition with 44.87% at 40 μM, indicating that the combination of a methyl group for steric effects and a nitro group for electron-withdrawing effects can enhance potency against tyrosinase.

Elongating the linker (**10o**) did not significantly enhance activity compared to compound (**10a**), suggesting that increased flexibility may not be advantageous for optimal binding to the enzyme's active site.

A study evaluating the inhibitory potency of cinnamic acid and triazole acetamide derivatives highlighted key SAR indicating that the presence of a phenolic hydroxyl group plays a crucial role in tyrosinase inhibition. Specifically, the *para*-hydroxyl group of compound **O** (Fig. 3) was shown to enhance inhibitory activity[39]. Another SAR analysis of cinnamic acid derivatives found that both the 4-OH and 4-F substitutions (compounds **P** and **Q**) significantly improved tyrosinase inhibition[15]. A comparative study of various cinnamic acid-based derivatives established the following order of activity: cinnamic acid > 2-hydroxycinnamic acid > 2-methoxycinnamic acid > 3-methoxycinnamic acid > 4-methoxycinnamic acid[40]. Further studies on heterocyclic compounds attached to cinnamic acid revealed that N-methylpiperazine (compound **R**) showed superior potency, particularly in B16F10 melanoma cell-based assays and in vitro testing[41]. Additionally, methoxylation and hydroxylation were found to play significant roles in modulating the tyrosinase inhibitory activity of cinnamic acid derivatives, as demonstrated in compound **S**[42]. The evaluation of triazole acetamides also revealed high potency against tyrosinase, with IC$_{50}$ values ranging from 0.11 to 0.79 μM and compound **T**, which features a 2-methyl-4-nitro substitution and exhibited 44.87 ± 6.66% inhibition at 40 μM[41]. Similar trends were seen in the current study in which derivative **10n** bearing 3-methyl-4-nitro exhibited better activity against tyrosinase (Fig. 3).

Kinetic studies of BChE inhibition

To determine the mechanism of inhibition, a kinetic study of **10j** as the most potent BChE inhibitor was done against BChE. The reciprocal Lineweaver–Burk plot (Fig. 4) illustrates that K_m and V_{max} reduced with the increasing concentration of inhibitor, which indicates that **10j** is a mix-type inhibitor.

Additionally, the plot of the slope of the lines versus different inhibitor concentrations gave an estimate of the inhibition constant (K_i) of 1.85 μM (Fig. 5a). Compound **10j** also recorded the inhibition constant with the enzyme-substrate complex (K_{is}) of 6.37 μM (Fig. 5b).

Docking study

In addition, an in silico study confirmed the inhibition of BChE. The first step of the docking study involved a validation method where the co-inhibitor was re-docked inside the binding pocket of BChE. The low root mean square deviation (RMSD) value for the re-docked complex with the crystallographic ligand exhibited an RMSD value of less than 2 Å, confirming the accuracy of the docking protocol.

BChE comprises several key regions including the peripheral anionic site, which consists of aspartic acid 70 and tyrosine 332, occupying the entrance of the active site. The catalytic binding site, located next to the peripheral anionic site, comprises tryptophan 82, where pi interactions with this residue are critical. The oxyanion hole, located in the middle of the BChE pocket, consists of glycine 116, glycine 117, and alanine 199.
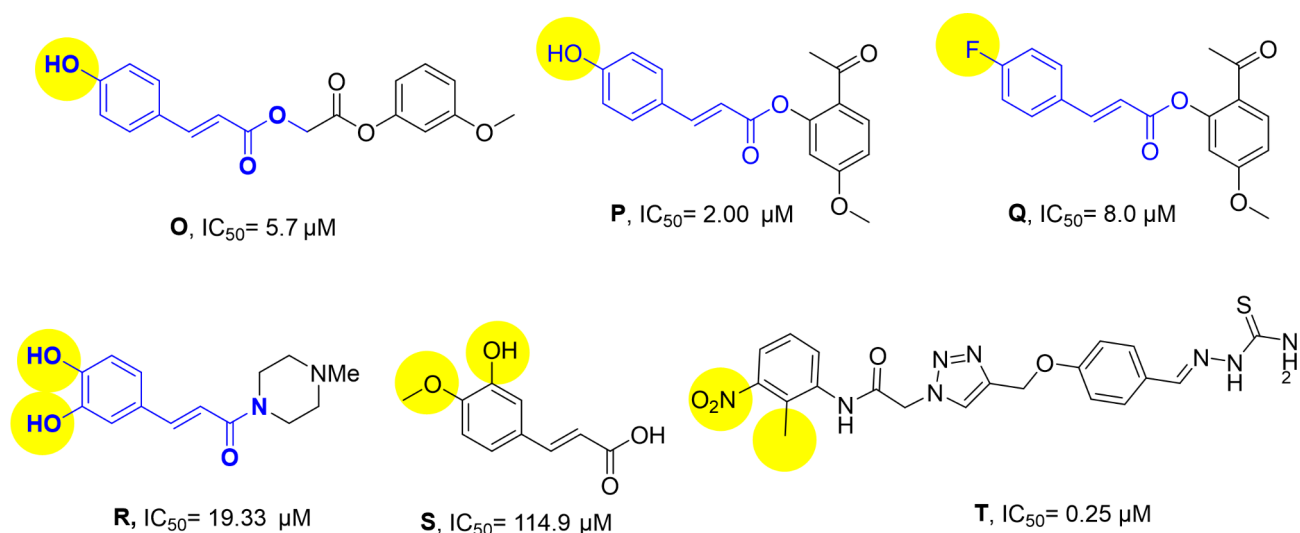

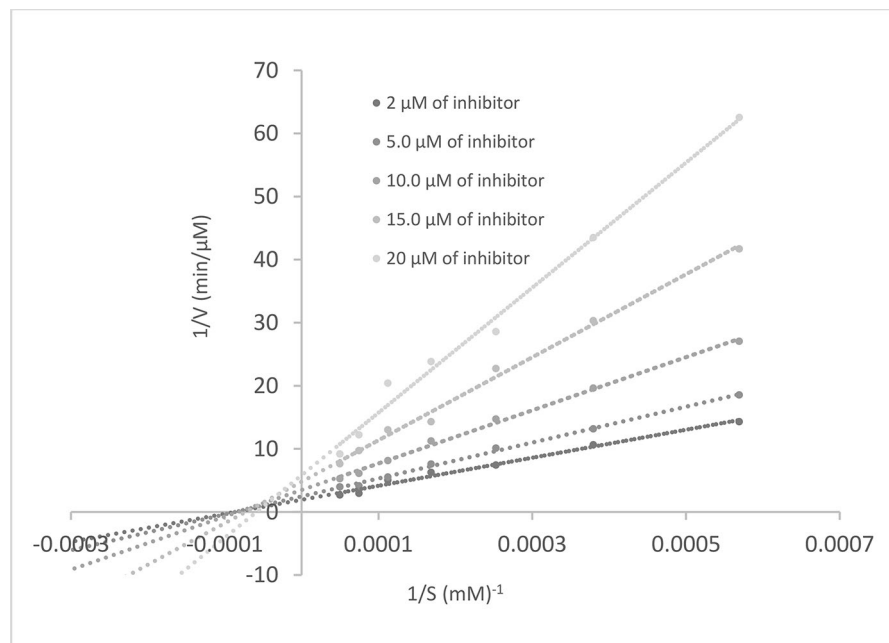**Fig. 3**. Comparision of SAR of previous studies related to tyrosinase.

Fig. 4. The Lineweaver–Burk plot of the most potent inhibitor **10j** at different concentrations against BChE.
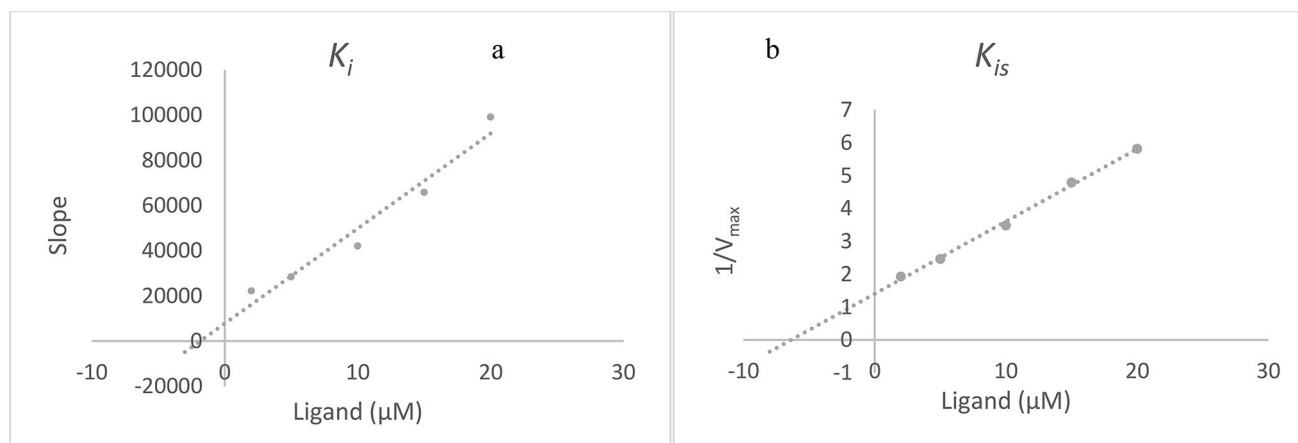

Fig. 5. (**a**) The secondary plot of slopes of the lines vs. various concentrations of **10j**; (**b**) The secondary plot of $1/V_{max}$ vs. various concentrations of **10j.**

The catalytic triad is comprised of serine 198, histidine 438, and glutamate 325. Interaction with these residues enhances the potency of the inhibitor.

Next, compound **10j** was docked against BChE. The results of the docking study for compound **10j** against BChE are shown in Fig. 6. The carboxyl group of cinnamic acid showed three hydrogen interactions with tyrosine 128, glycine 116, and glutamate 197. The methoxyphenyl group of the cinnamic acid ring exhibited pi-pi stacking interactions with tryptophan 82. The triazole moiety showed pi-pi stacking interactions with tyrosine 332. Finally, the terminal acetamide showed hydrogen bond interactions with proline 285. Overall, the in-silico docking study provides a powerful, efficient, and cost-effective approach identifying and optimizing BChE inhibitors, contributing significantly to the field of drug discovery and development.

Molecular dynamics simulations

To evaluate the stability and flexibility of the **10j**-BChE complex, molecular dynamics simulations were carried out. For comparison, the dynamics of the BChE enzyme alone were also simulated under similar conditions.

In this study, the apoenzyme was monitored across three different phases over a 20 ns period, during which the RMSD gradually increased to 1.5 Å. Stability was then observed up to 75 ns, followed by a further increase to 2 Å, which remained constant until the end of the simulation. The **10j**-BChE complex exhibited a similar behavior up to 50 ns. However, beyond this point, the complex showed a sharp decrease in RMSD to 1.25 Å,
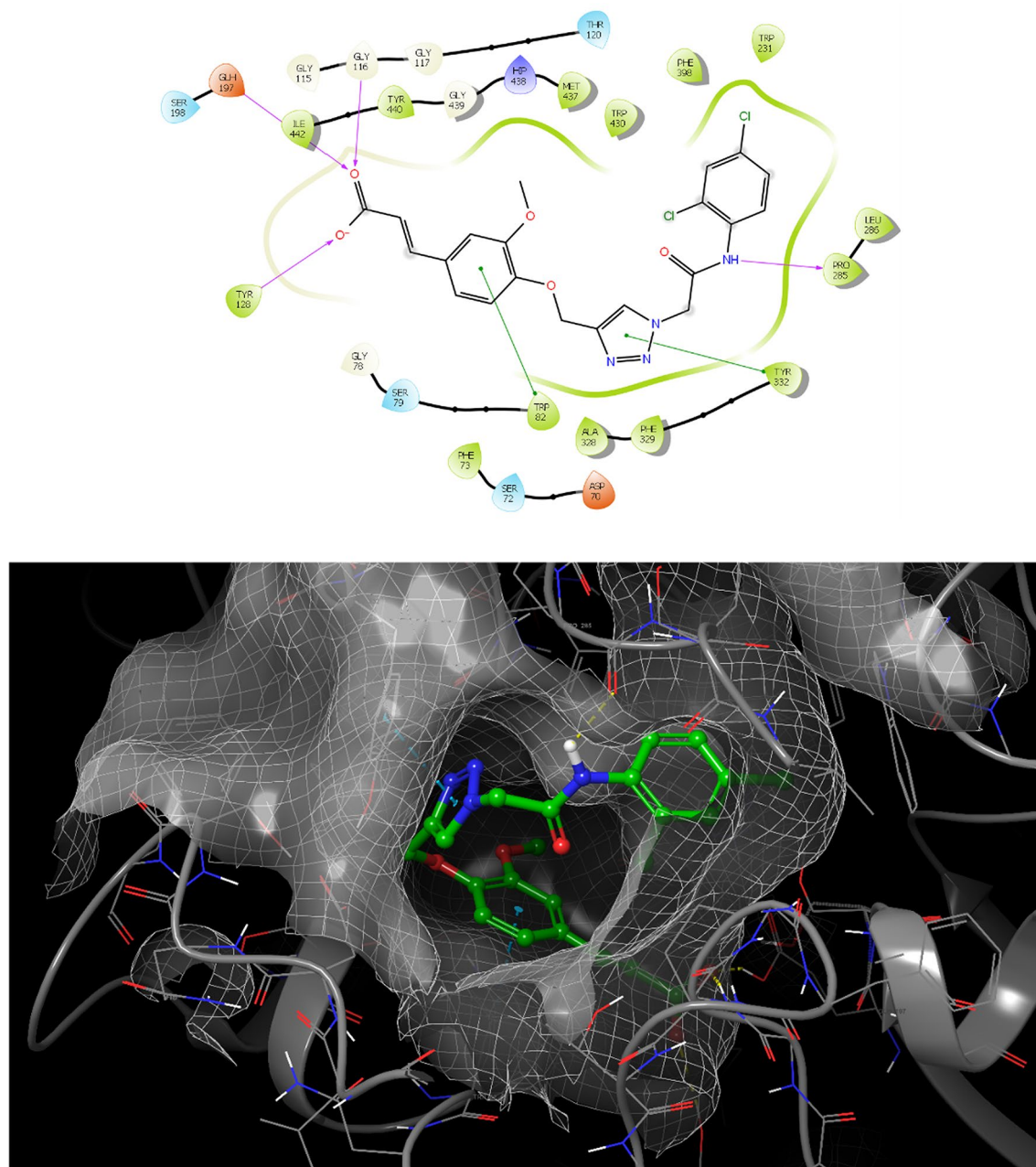
Fig. 6. 2D and 3D interaction of **10j** in the BChE active site.

which was maintained until 75 ns. This was followed by another decrease to an RMSD value of 1 Å, indicating strong stability of the **10j**-BChE complex during the MD simulation (Fig. 7).

Additionally, the root mean square fluctuation (RMSF) of the backbone atoms in BChE and **10j**-BChE were computed to assess the flexibility of the enzyme's residues and the ligand's atoms. As shown in Fig. 8, different regions of this apoprotein exhibit varying degrees of fluctuation. Specifically, higher fluctuations were observed in the residues located in the PAS pocket regions. The catalytic triad, consisting of serine 198, histidine 438, and glutamate 325, also showed high fluctuation (Fig. 8).

However, these regions showed lower RMSF values when interacting with **10j**. Specifically, the terminal COOH group of **10j** engaged in multiple interactions with the oxyanion hole, formed by glycine 116, glycine 117, and alanine 199, leading to a reduction in RMSF in this area. Additionally, the terminal COO group and the 2,4-dichlorophenyl group of **10j** were involved in interactions with the catalytic triad (serine 198, histidine 438, and glutamate 325), further emphasizing their significance in catalytic activity and their role in stabilizing the protein through interactions with the terminal COOH group of cinnamic acid.

This pattern suggests a stable protein structure, particularly in the critical areas involved in catalytic function and ligand interaction.
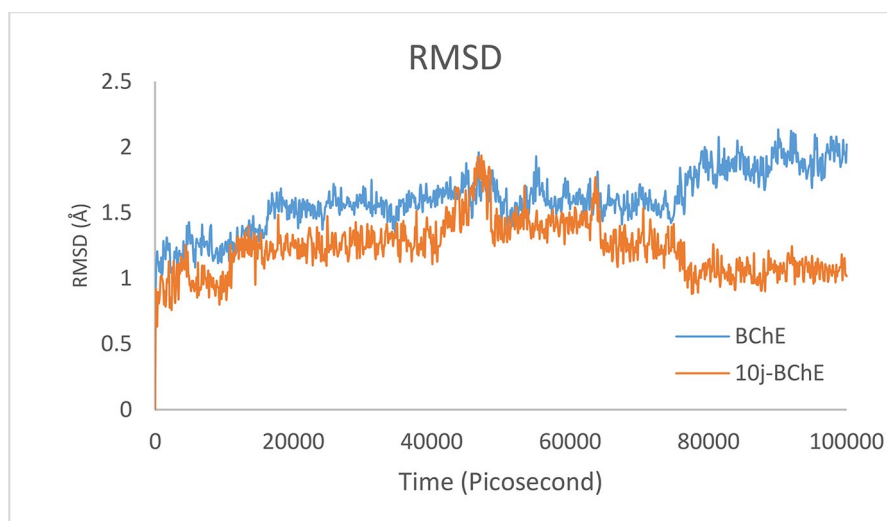
Fig. 7. The RMSD of **10j**-BChE *vs*. BChE during 100 nanosecond molecular dynamics simulations.
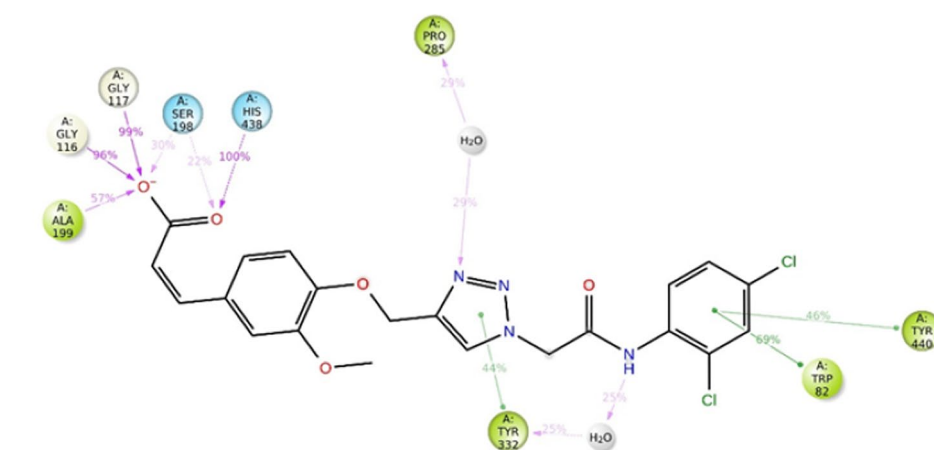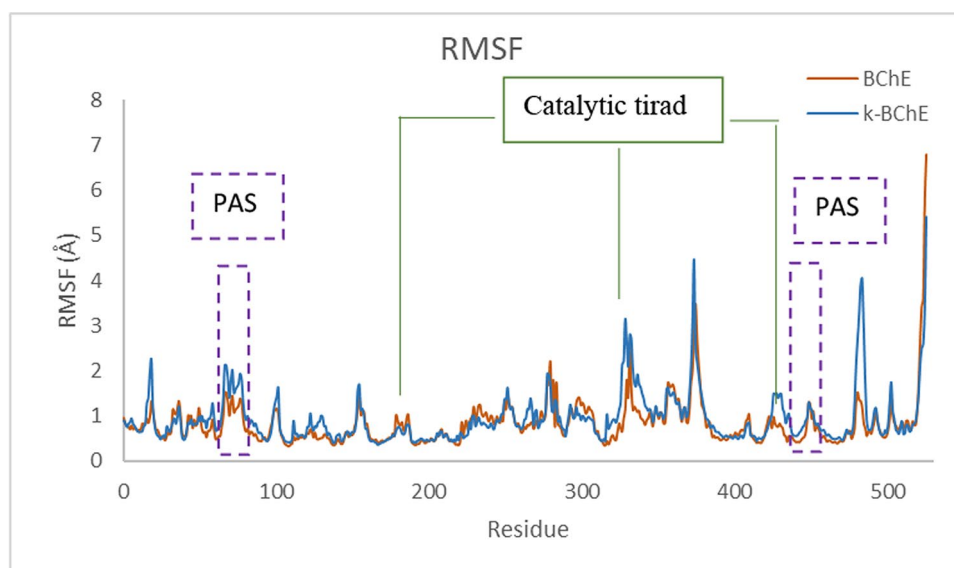

Fig. 8. (**a**) RMSF graph of the Cα atoms of **10j** -BChE and BChE and (**b**) representation of **10j**-BChE Interactions that happened for over 30% of the simulation.
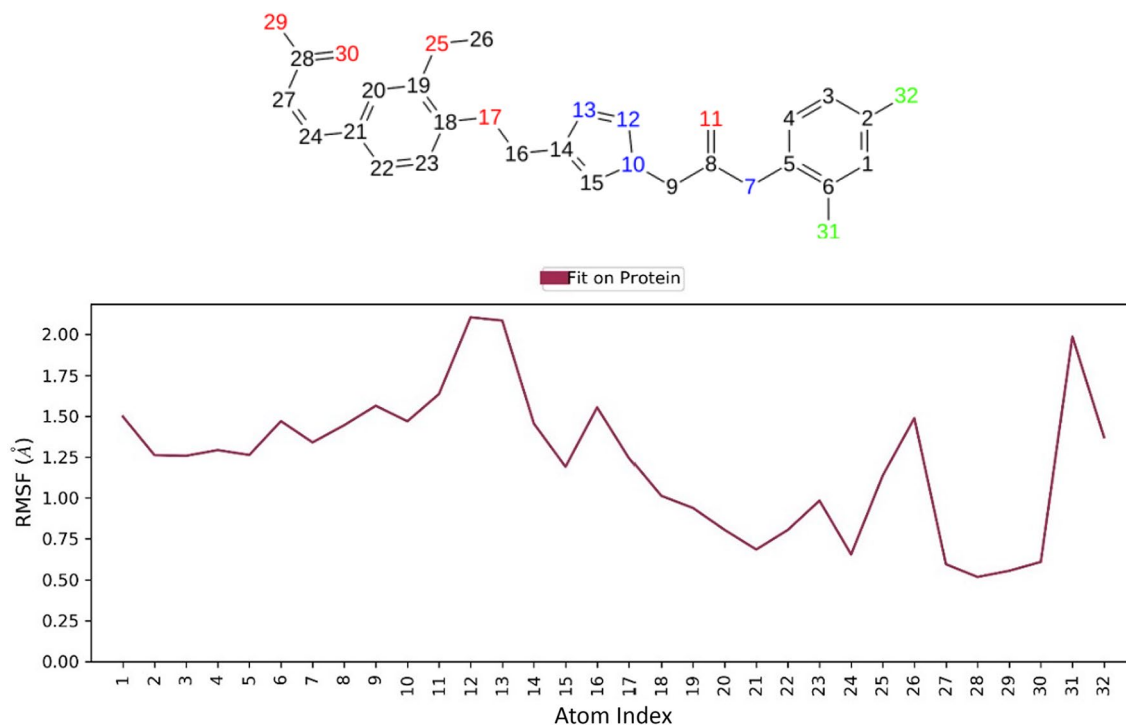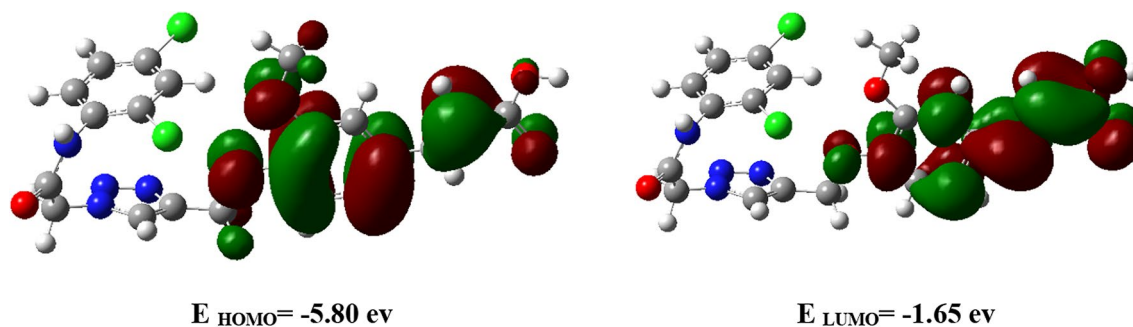
Fig. 9. RMSF graph of **10j** in the active site.

E _HOMO_= -5.80 ev   E _LUMO_= -1.65 ev

Fig. 10. DFT calculated HOMO, LUMO, and their energies for **10j**, (Gaussian version 09; https://gaussian.com/glossary/g09/)

As expected, the RMSF of all heavy atoms in **10j** remained below 2 Å, except for atoms 12 and 13, which maintained a fluctuation of around 2 Å. This minimal fluctuation suggests stable complexation between the ligand and BChE, indicating that the movements of **10j** are constrained by strong intermolecular interactions (Fig. 9).

DFT analysis

For enzyme inhibition, understanding the electron distribution within a molecule is critical. Density Functional Theory (DFT) analysis offers valuable insights into the electronic properties of compounds, which directly influence their interactions with enzyme active sites and thus their inhibitory potential. In enzyme inhibition studies, DFT is often used to calculate molecular parameters such as HOMO (highest occupied molecular orbital) and LUMO (lowest unoccupied molecular orbital) energies, the HOMO-LUMO gap, and electrostatic potential (ESP). These parameters can indicate a compound's reactivity, stability, and preferred interaction sites with enzymes.

As a result, in the current study, DFT was applied to calculate the HOMO and LUMO energies, as well as the HOMO-LUMO energy gap for compound **10j** using the B3LYP/6-31G(d, p) method (Fig. 10). These calculated values provide valuable insights into the compound's reactivity, stability, and physical and structural characteristics. In the molecular orbital diagrams, the red regions represent the positive phase, while the green regions represent the negative phase. Compound **10j** exhibits a consistent distribution of HOMO and LUMO
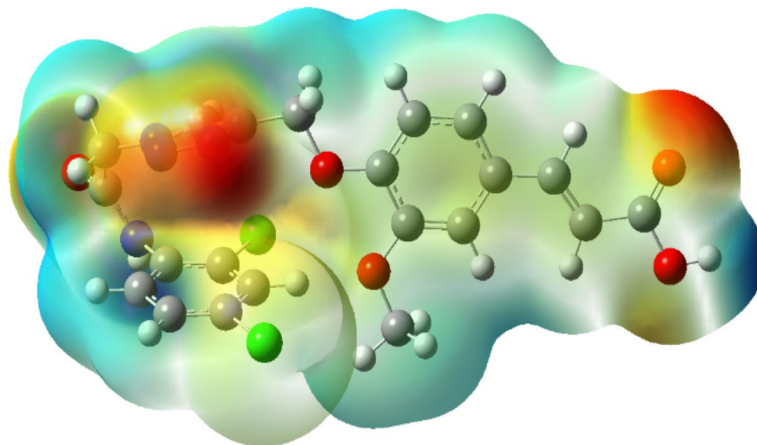
Fig. 11. ESP maps for **10j** at B3LYP/6–31 + G (d, p) level of theory (GaussView version 6.0; https://gaussian.com/gaussview6/).

Compound	Log *P*	HBD	HBA	MW	RB	PSA
10a	2.6022	2	7	408.414	9	172.100
10b	2.9106	2	7	422.441	9	178.465
10c	2.9106	2	7	422.441	9	178.465
10d	2.9106	2	7	422.441	9	178.465
10e	2.3078	2	7	424.413	9	176.894
10f	2.7413	2	7	426.404	9	176.266
10g	3.2556	2	7	442.859	9	182.403
10h	3.2556	2	7	442.859	9	182.403
10i	3.2556	2	7	442.859	9	182.403
10j	3.909	2	7	477.304	9	192.707
10k	2.5104	2	9	453.411	10	186.753
10l	2.5104	2	9	453.411	10	186.753
10m	2.5104	2	9	453.411	10	186.753
10n	2.8188	2	9	467.438	10	193.118
10o	2.3224	2	7	436.468	11	184.830

Table 2. Physicochemical properties of the synthesized compounds.

orbitals, with the HOMO primarily localized on the methoxyphenyl group and the LUMO on the cinnamic acid moiety. The calculated energy gap for compound **10j** is − 4.15 eV, indicating increased reactivity.

Figure 11 presents the ESP map for compound **10j**, where blue, red, and green represent positive, negative, and neutral regions, respectively. As shown in the figure, electronegative groups, such as hydroxyl and carbonyl, are situated in the red areas. Overall, the ESP map for the studied compounds indicates a well-distributed electron cloud, which is likely to enhance their interactions with biological enzymes.

Pharmacokinetic properties

The online tool PKCSM was utilized to assess the physicochemical properties and ADME-T characteristics of the synthesized compounds, with the findings detailed in Tables 2 and 3. The Polar Surface Area (PSA) values ranged from approximately 172.1 to 193.1 Å², which plays a crucial role in influencing permeability and absorption. The molecular weights (MW) of the compounds varied from 408.41 to 477.30 g/mol, which fall within an acceptable range for drug-like properties. Most compounds exhibited 7 hydrogen bond acceptors (HBA) and 2 hydrogen bond donors (HBD), indicating a balance that can affect solubility and interactions with biological targets. Log P values ranged from 2.31 to 3.91, reflecting variations in lipophilicity that influence membrane permeability and absorption characteristics.

The predicted intestinal absorption rates for the synthesized compounds are approximately 68% for most, indicating a favorable profile for oral administration. Additionally, the Caco-2 permeability values, ranging from about 0.026 to 1.324, provide insights into the compounds' potential for intestinal absorption, with higher values suggesting enhanced permeability. The Volume of Distribution at Steady State (VDss) reflects the extent to which compounds distribute into body tissues relative to plasma, which is critical for understanding their pharmacokinetics. Moreover, the assessment of cytochrome P450 enzyme inhibition is essential, as these

Compound	Intestinal absorption (human)	Caco2 permeability	VDss (human)	CYP2C19 inhibitor	CYP2C9 inhibitor	CYP2D6 inhibitor	CYP3A4 inhibitor	Total clearance	Oral rat acute toxicity (LD50)
10a	67.024	1.324	− 0.999	No	Yes	No	No	0.368	2.458
10b	67.492	0.793	− 0.954	No	Yes	No	No	0.377	2.511
10c	72.63	0.793	− 0.971	No	Yes	No	No	0.373	2.513
10d	72.63	0.793	− 0.971	No	Yes	No	No	0.373	2.513
10e	61.588	0.254	− 0.564	No	Yes	No	No	0.213	2.552
10f	62.968	0.788	− 1.074	No	Yes	No	No	0.026	2.489
10g	68.2	0.785	− 0.997	No	Yes	No	No	0.133	2.545
10h	73.338	0.785	− 1.013	No	Yes	No	No	− 0.074	2.547
10i	73.338	0.768	− 1.013	No	Yes	No	No	− 0.135	2.544
10j	74.514	0.763	− 1.006	No	Yes	No	No	0.058	2.619
10k	69.085	− 0.200	− 1.263	No	Yes	No	No	0.107	2.255
10l	69.117	− 0.236	− 1.264	No	Yes	No	No	0.209	2.261
10m	66.111	− 0.24	− 1.281	No	Yes	No	No	0.202	2.263
10n	66.611	− 0.151	− 1.203	No	Yes	No	No	0.218	2.255
10o	68.862	0.789	− 1.028	No	Yes	No	No	0.563	2.328

Table 3. ADME[a] prediction of the synthesized compounds.

enzymes significantly impact drug metabolism. The total clearance values range from 0.026 to 0.563 L/hr/kg, illustrating the variability in how efficiently each compound is processed and eliminated from the body. Finally, the oral rat acute toxicity (LD_{50}) values, ranging from approximately 2.255 to 2.619 g/kg, provide estimates of the lethal dose required to kill 50% of a test population of rats upon oral administration, indicating varying levels of toxicity among the compounds.

Conclusion

In this study, we synthesized a series of cinnamic acid derivatives linked to triazole acetamide and evaluated their inhibitory effects on AChE, BChE, and tyrosinase. Our results showed that the introduction of methyl groups significantly influenced AChE inhibitory activity, with the 4-CH_3 substitution demonstrating the highest potency due to an optimal balance of steric and electronic effects. In contrast, *ortho* substitutions, like 2-ethyl, reduced activity due to increased steric hindrance. For BChE, the 2,4-diCl substituted derivative (**10j**, $IC_{50} = 11.99 \pm 0.53$ μM) was the most active, highlighting that bulkier, electron-withdrawing groups enhance inhibition. Kinetic studies indicated mixed-type inhibition and in silico studies confirmed interactions with key enzyme residues affecting potency. Tyrosinase inhibition was optimized and compound **10n** yielded the highest inhibition, demonstrating the beneficial balance of steric and electronic effects. Compared to similar studies, our findings align with previous research on cinnamic acid derivatives as effective inhibitors, while our exploration of triazole acetamide conjugation enhances the understanding of SAR. This study contributes novel insights into the multi-target inhibition profile of these derivatives, which were less frequently addressed in the literature. Our study presents two significant aspects. We identified a range of diverse derivatives with strong enzyme inhibition potential, which could be useful for developing new treatments for neurodegenerative diseases. Second, we provide important insights that will guide future drug design efforts.

Method and materials
General procedure for the synthesis of 10a-o

Initially, 4-hydroxy-3-methoxybenzaldehyde **1** (1 mmol) was added to K_2CO_3 (1.1 mmol) in DMF (3 mL). To the stirring solution, propargyl bromide **2** (1.1 mmol) was added dropwise. The reaction mixture was stirred at room temperature for 12 h. The progress of the reaction was monitored by thin-layer chromatography (TLC) until completion. Upon completion, the reaction mixture was quenched with water (10 mL), yielding the desired precipitate of compound **3**[43,44].

Subsequently, a mixture of aniline derivatives (**4a–o**) (2 mmol) and chloroacetyl chloride[5] (2 mmol) in acetone (10 mL) was stirred at room temperature for 30 min. The reaction mixture was then diluted with cold water and poured onto ice. The resulting precipitate was filtered, washed with cold water, and dried to afford pure N-phenyl-2-chloroacetamides (**6a–o**)[45].

Various organic azides (**7a–o**) were synthesized by reacting different N-phenyl acetamides (**6a–n**) with sodium azide in the presence of triethylamine (Et_3N) in a mixture of H_2O/t-BuOH at room temperature. Following this, compound **3**, sodium ascorbate, and a catalytic amount of $CuSO_4·5 H_2O$ (7 mol%) were added to the freshly prepared azides (**7a–o**), leading to the formation of 1,2,3-triazoles (**8a–o**)[44].

A mixture of malonic acid (**8**, 12 mmol), compound **9a–o** (10 mmol), piperidine (15 mmol), and pyridine (0.3 mmol) was stirred under reflux for 3 h, with progress monitored by TLC. After the solvent was removed under vacuum, the residue was poured into ice water, and the pH was adjusted to 2 using 10% HCl. The resulting

precipitate was filtered, thoroughly washed with H_2O, recrystallized using 95% ethanol, and dried under vacuum to afford the final products (**10a–o**)[46].

(E)-3-(3-Methoxy-4-((1-(2-oxo-2-(phenylamino)ethyl)-1H-1,2,3-triazol-4-yl)methoxy)phenyl)acrylic acid (10a)
Brown solid; Yield:84%;MP = 178–180 °C; IR (KBr, v_{max}) 3210 (NH), 3020 (CH Aromatic), 2920 (CH Aliphatic), 1664 (C=O) Cm^{-1}; ^1H NMR (499 MHz, DMSO-d_6) δ 12.19 (s, 1H, OH_{Acid}), 10.47 (s, 1H, NH_{Amide}), 8.26 (s, 1H, H Ar), 7.57 (d, J = 8.0 Hz, 2 H, H Ar), 7.52 (d, J = 15.9 Hz, 1H, H $_{Olefinic}$), 7.36–7.28 (m, 3 H, H Ar), 7.20 (s, 2 H, H Ar), 7.07 (t, J = 7.6 Hz, 1H, H Ar), 6.45 (d, J = 16.0 Hz, 1H, H $_{Olefinic}$), 5.35 (s, 2 H, CH_2), 5.19 (s, 2 H, CH_2), 3.79 (s, 3 H, $CH_{3\ Methoxy}$); ^{13}C NMR (126 MHz, DMSO-d_6) δ 168.36, 164.63, 149.89, 149.60, 144.48, 142.64, 138.86, 129.37, 127.95, 126.97, 124.24, 122.88, 119.68, 117.45, 113.45, 111.00, 61.95, 56.00, 52.67; ESI-MS ($C_{21}H_{20}N_4O_5$): calculated m/z 408.14 M^+, observed m/z 409.04 M^+; Anal. Calcd: $C_{21}H_{20}N_4O_5$; C, 61.76; H, 4.94; N, 13.72; Found; C, 61.93; H, 5.10; N, 13.91.

(E)-3-(3-Methoxy-4-((1-(2-oxo-2-(o-tolylamino)ethyl)-1H-1,2,3-triazol-4-yl)methoxy)phenyl)acrylic acid (10b)
Cream solid; Yield:65%;MP = 187–189 °C; IR (KBr, v_{max}) 3225 (NH), 3015 (CH Aromatic), 2930 (CH Aliphatic), 1666 (C=O) Cm^{-1} ^1H NMR (499 MHz, DMSO-d_6) δ 9.88 (s, 1 H, NH_{Amide}), 8.25 (s, 1 H, H Ar), 7.52 (d, J = 15.8 Hz, 1 H, H $_{Olefinic}$), 7.41 (d, J = 7.9 Hz, 1 H, H Ar), 7.30 (s, 1 H, H Ar), 7.23–7.18 (m, 3 H, H Ar), 7.15 (t, J = 7.6 Hz, 1 H, H Ar), 7.09 (t, J = 7.4 Hz, 1 H, H Ar), 6.44 (d, J = 15.9 Hz, H $_{Olefinic}$), 5.41 (s, 2 H, CH_2), 5.18 (s, 2 H, CH_2), 3.77 (s, 3 H, $CH_{3\ Methoxy}$), 2.22 (s, 3 H, $CH_{3\ Methyl}$) ^{13}C NMR (126 MHz, DMSO-d_6) δ 168.34, 164.83, 149.89, 149.59, 144.53, 142.62, 135.95, 132.11, 130.89, 127.92, 126.95, 126.51, 126.04, 125.22, 122.88, 117.37, 113.46, 110.99, 61.93, 56.00, 55.98, 52.39, 18.27; ESI-MS ($C_{22}H_{22}N_4O_5$): calculated m/z 422.16 M^+, observed m/z 423.13 M^+; Anal. Calcd: $C_{22}H_{22}N_4O_5$; C, 62.55; H, 5.25; N, 13.26; Found; C, 62.72; H, 5.44 N, 13.47.

(E)-3-(3-Methoxy-4-((1-(2-oxo-2-(m-tolylamino)ethyl)-1H-1,2,3-triazol-4-yl)methoxy)phenyl)acrylic acid (10c)
Cream solid; Yield:64%;MP = 169-172-207 °C; IR (KBr, v_{max}) 3220 (NH), 3030 (CH Aromatic), 2940 (CH Aliphatic), 1662 (C=O) Cm^{-1}; ^1H NMR (499 MHz, DMSO-d_6) δ 12.20 (s, 1H, OH_{Acid}), 10.40 (s, 1H, NH_{Amide}), 8.25 (s, 1H, H Ar), 7.53 (d, J = 15.9 Hz, 1H, H $_{Olefinic}$), 7.41 (s, 1H, H Ar), 7.36 (d, J = 8.1 Hz, 1H, H Ar), 7.32 (s, 1H, H Ar), 7.23–7.17 (m, 3 H, H Ar), 6.89 (d, J = 7.5 Hz, 1H, H Ar), 6.45 (d, J = 16.0 Hz, 1H, H $_{Olefinic}$), 5.33 (s, 2 H, CH_2), 5.19 (s, 2 H, CH_2), 3.79 (s, 3 H, $CH_{3\ Methoxy}$), 2.26 (s, 3 H, $CH_{3\ Methyl}$); ^{13}C NMR (126 MHz, DMSO-d_6) δ 168.33, 164.55, 149.91, 149.60, 144.53, 142.63, 138.78, 138.59, 129.20, 127.93, 126.96, 124.94, 122.90, 120.23, 117.38, 116.87, 113.43, 111.00, 61.94, 55.99, 52.68, 21.61; ESI-MS ($C_{22}H_{22}N_4O_5$): calculated m/z 422.16 M^+, observed m/z 423.14 M^+; Anal. Calcd: $C_{22}H_{22}N_4O_5$; C, 62.55; H, 5.25; N, 13.26; Found; C, 62.73; H, 5.41; N, 13.43.

(E)-3-(3-Methoxy-4-((1-(2-oxo-2-(p-tolylamino)ethyl)-1H-1,2,3-triazol-4-yl)methoxy)phenyl)acrylic acid (10d)
Cream solid; Yield:69%; MP = 185–187 °C; IR (KBr, v_{max}) 3235 (NH), 3015 (CH Aromatic), 2930 (CH Aliphatic), 1665 (C=O) Cm^{-1} ^1H NMR (499 MHz, DMSO-d_6) δ 10.43 (s, 1 H, NH_{Amide}), 8.24 (s, 1 H, H Ar), 7.49–7.43 (m, 3 H, H Ar, H $_{Olefinic}$), 7.27 (s, 1 H, H Ar), 7.17 (s, 2 H, H Ar), 7.12 (d, J = 8.0 Hz, 2 H, H Ar), 6.43 (d, J = 15.9 Hz, 1 H, H $_{Olefinic}$), 5.32 (s, 2 H, CH_2), 5.17 (s, 2 H, CH_2), 3.78 (s, 3 H, $CH_{3\ Methoxy}$), 2.24 (s, 3 H, $CH_{3\ Methyl}$); ^{13}C NMR (126 MHz, DMSO-d_6) δ 164.36, 157.15, 149.59, 142.66, 136.37, 135.05, 133.20, 131.46, 129.73, 128.36, 126.93, 122.50, 119.68, 113.50, 110.86, 110.72, 61.96, 55.94, 52.64, 20.89; ESI-MS ($C_{22}H_{22}N_4O_5$): calculated m/z 422.16 M^+, observed m/z 423.10 M^+; Anal. Calcd: $C_{22}H_{22}N_4O_5$; C, 62.55; H, 5.25; N, 13.26; Found; C, 62.74; H, 5.43; N, 13.41.

(E)-3-(4-((1-(2-((4-Hydroxyphenyl)amino)-2-oxoethyl)-1H-1,2,3-triazol-4-yl)methoxy)-3-methoxyphenyl)acrylic acid (10e)
Cream solid; Yield:61%; MP = 181–183 °C; IR (KBr, v_{max}) 3270 (NH), 3030 (CH Aromatic), 2935 (CH Aliphatic), 1669 (C=O) Cm^{-1}; ^1H NMR (499 MHz, DMSO-d_6) δ 12.20 (s, 1H), 10.25 (s, 1H), 9.26 (s, 1H, H Ar), 8.23 (s, 1H, H Ar), 7.52 (d, J = 15.9 Hz, 1H, H $_{Olefinic}$), 7.35 (d, J = 8.7 Hz, 2 H, H Ar), 7.31 (s, 1H, H Ar), 7.21–7.18 (m, 2 H, H Ar), 6.70 (d, J = 8.9 Hz, 2 H, H Ar), 6.44 (d, J = 15.9 Hz, 1H, H $_{Olefinic}$), 5.28 (s, 2 H, CH_2), 5.18 (s, 2 H, CH_2), 3.78 (s, 3 H, $CH_{3\ Methoxy}$); ^{13}C NMR (126 MHz, DMSO-d_6) δ 168.31, 163.83, 154.18, 149.91, 149.59, 144.53, 142.58, 130.46, 127.91, 126.91, 122.90, 121.43, 117.36, 115.67, 113.44, 110.99, 61.94, 56.01, 52.58; Anal. Calcd: $C_{21}H_{20}N_4O_6$: C, 59.43; H, 4.75; N, 13.20; Found; C, 59.58; H, 4.81; N, 13.35.

(E)-3-(4-((1-(2-((4-Fluorophenyl)amino)-2-oxoethyl)-1H-1,2,3-triazol-4-yl)methoxy)-3-methoxyphenyl) acrylic acid (10f)
Cream solid; Yield:67%; MP = 175–177 °C; IR (KBr, v_{max}) 3240 (NH), 3020 (CH Aromatic), 2920 (CH Aliphatic), 1666 (C=O) Cm^{-1}; ^1H NMR (499 MHz, DMSO-d_6) δ 12.20 (s, 1H, OH_{Acid}), 10.53 (s, 1H, NH_{Amide}), 8.25 (s, 1H, H Ar), 7.59 (dd, J = 7.2, 4.9 Hz, 2 H, H Ar), 7.52 (d, J = 16.8 Hz, 1H, H $_{Olefinic}$), 7.32 (s, 1H, H Ar), 7.22–7.14 (m, 4 H, H Ar), 6.44 (d, J = 15.9 Hz, 1H, H $_{Olefinic}$), 5.34 (s, 2 H, CH_2), 5.19 (s, 2 H, CH_2), 3.78 (s, 3 H, $CH_{3\ Methoxy}$): ^{13}C NMR (126 MHz, DMSO-d_6) δ 168.32, 164.58, 157.74, 149.90, 149.60, 144.53, 142.65, 135.25, 127.93, 126.96, 122.90, 121.52, 121.46, 117.37, 116.06, 115.88, 113.45, 111.00, 61.94, 56.01, 52.59; ESI-MS ($C_{21}H_{19}FN_4O_5$): calculated m/z 426.13 M^+, observed m/z 427.06 M^+; Anal. Calcd: $C_{21}H_{19}FN_4O_5$; C, 59.15; H, 4.49; N, 13.14; Found; C, 59.33; H, 4.67; N, 13.35.

(E)-3-(4-((1-(2-((2-Chlorophenyl)amino)-2-oxoethyl)-1H-1,2,3-triazol-4-yl)methoxy)-3-methoxyphenyl)acrylic acid (10 g)
Brown solid; Yield:75%; MP = 182–184 °C; IR (KBr, v_{max}) 3260 (NH), 3040 (CH Aromatic), 2930 (CH Aliphatic), 1669 (C=O) Cm^{-1}; ^1H NMR (499 MHz, DMSO-d_6) δ 12.21 (s, 1H, OH_{Acid}), 10.07 (s, 1H, NH_{Amide}), 8.25 (s,

1H, H Ar), 7.74 (d, $J = 7.9$ Hz, 1H, H Ar), 7.55–7.49 (m, 2 H, H Ar, H $_{Olefinic}$), 7.32 (d, $J = 5.9$ Hz, 2 H, H Ar), 7.24–7.16 (m, 3 H, H Ar), 6.45 (d, $J = 15.8$ Hz, 1H, H $_{Olefinic}$), 5.46 (s, 2 H, CH$_2$), 5.19 (s, 2 H, CH$_2$), 3.78 (s, 3 H, CH$_{3\ Methoxy}$); ^{13}C NMR (126 MHz, DMSO-d_6) δ 168.34, 165.34, 149.89, 149.60, 144.50, 142.68, 134.61, 130.08, 128.01, 127.95, 127.18, 127.00, 126.74, 126.34, 122.89, 117.42, 113.46, 111.00, 61.94, 56.01, 55.99, 52.39; ESI-MS (C$_{21}$H$_{19}$ClN$_4$O$_5$): calculated m/z 442.10 M$^+$, observed m/z 443.08 M$^+$; Anal. Calcd: C$_{21}$H$_{19}$ClN$_4$O$_5$; C, 56.96; H, 4.32; N, 12.65; Found: C, 57.12; H, 4.47; N, 12.82.

*(E)-3-(4-((1-(2-((3-Chlorophenyl)amino)-2-oxoethyl)-1H-1,2,3-triazol-4-yl)methoxy)-3-methoxyphenyl)acrylic acid (**10 h**)*
Berown solid; Yield:72%; MP = 175–177 ºC; IR (KBr, v$_{max}$) 3230 (NH), 3010 (CH Aromatic), 2940 (CH Aliphatic), 1661 (C=O) Cm^{-1}; ^{1}H NMR (499 MHz, DMSO-d_6) δ 12.20 (s, 1H, OH$_{Acid}$), 10.07 (s, 1H, NH$_{Amide}$), 8.25 (s, 1H, H Ar), 7.74 (d, $J = 8.1$ Hz, 1H, H Ar), 7.55–7.48 (m, 2 H, H Ar, H $_{Olefinic}$), 7.36–7.29 (m, 2 H, H Ar), 7.23–7.16 (m, 3 H, H Ar), 6.45 (d, $J = 15.9$ Hz, 1H, H $_{Olefinic}$), 5.46 (s, 2 H, CH$_2$), 5.19 (s, 2 H, CH$_2$), 3.78 (s, 3 H, CH$_{3\ Methoxy}$); ^{13}C NMR (126 MHz, DMSO-d_6) δ 168.34, 165.34, 149.89, 149.60, 144.50, 142.68, 134.61, 130.08, 128.01, 127.95, 127.18, 127.00, 126.74, 126.33, 122.89, 117.42, 113.46, 111.00, 61.94, 56.00, 52.39; ESI-MS (C$_{21}$H$_{19}$ClN$_4$O$_5$): calculated m/z 442.10 M$^+$, observed m/z 443.06 M$^+$; Anal. Calcd: C$_{21}$H$_{19}$ClN$_4$O$_5$; C, 56.96; H, 4.32; N, 12.65; Found: C, 57.10; H, 4.51; N, 12.82.

*(E)-3-(4-((1-(2-((4-Chlorophenyl)amino)-2-oxoethyl)-1H-1,2,3-triazol-4-yl)methoxy)-3-methoxyphenyl)acrylic acid (**10i**)*
Cream solid; Yield:78%; MP = 187–189 ºC; IR (KBr, v$_{max}$) 3255 (NH), 3045 (CH Aromatic), 2935 (CH Aliphatic), 1668 (C=O) Cm^{-1} ^{1}H NMR (499 MHz, DMSO-d_6) δ 12.20 (s, 1 H, OH$_{Acid}$),10.61 (s, 1 H, NH$_{Amide}$), 8.25 (s, 1 H, H Ar), 7.59 (d, $J = 8.4$ Hz, 2 H, H Ar), 7.55–751 (m, 1 H, H $_{Olefinic}$), 7.38 (d, $J = 8.6$ Hz, 2 H, H Ar), 7.31 (s, 1 H, H Ar), 7.21–7.18 (m, 2 H, H Ar), 6.44 (d, $J = 15.9$ Hz, 1 H, H $_{Olefinic}$), 5.35 (s, 2 H, CH$_2$), 5.19 (s, 2 H, CH$_2$), 3.78 (s, 3 H, CH$_{3\ Methoxy}$); δ ^{13}C NMR (126 MHz, DMSO-d_6) δ 168.86, 164.85, 149.88, 149.60, 144.45, 143.03, 141.38, 133.99, 129.31, 127.95, 127.03, 122.88, 121.25, 117.25, 113.45, 110.99, 61.93, 56.00, 52.63.; Anal. Calcd: C$_{21}$H$_{19}$ClN$_4$O$_5$; C, 56.96; H, 4.32; N, 12.65; Found; C, 57.12; H, 4.48; N, 12.87.

*(E)-3-(4-((1-(2-((2,4-Dichlorophenyl)amino)-2-oxoethyl)-1H-1,2,3-triazol-4-yl)methoxy)-3-methoxyphenyl) acrylic acid (**10j**)*
Brown solid; Yield:71%; MP = 198–200 ºC; IR (KBr, v$_{max}$) 3250 (NH), 3065 (CH Aromatic), 2940 (CH Aliphatic), 1669 (C=O) Cm^{-1} ^{1}H NMR (499 MHz, DMSO-d_6) δ 12.20 (s, 1 H, OH$_{Acid}$), 10.21 (s, 1 H, NH$_{Amide}$), 8.25 (s, 1 H, H Ar), 7.76 (d, $J = 8.7$ Hz, 1 H, H Ar), 7.68 (d, $J = 2.5$ Hz, 1 H, H Ar), 7.52 (d, $J = 16.0$ Hz, 1 H, H $_{Olefinic}$), 7.41 (dd, $J = 8.7, 2.5$ Hz, 1 H, H Ar), 7.31 (s, 1 H, H Ar), 7.22–7.16 (m, 2 H, H Ar), 6.44 (d, $J = 15.9$ Hz, 1 H, H $_{Olefinic}$), 5.47 (s, 2 H, CH$_2$), 5.19 (s, 2 H, CH$_2$), 3.78 (s, 3 H, CH$_{3\ Methoxy}$); ^{13}C NMR (126 MHz, DMSO-d_6) δ 168.33, 165.52, 149.88, 149.60, 144.48, 142.68, 133.85, 130.26, 129.53, 128.15, 127.95, 127.66, 127.33, 127.00, 124.19, 122.87, 117.43, 113.46, 61.93, 55.99, 52.38; Anal. Calcd: C$_{21}$H$_{18}$Cl$_2$N$_4$O$_5$: C, 52.85; H, 3.80; N, 11.74; Found; C, 52.98; H, 3.98; N, 11.96.

*(E)-3-(3-Methoxy-4-((1-(2-((2-nitrophenyl)amino)-2-oxoethyl)-1H-1,2,3-triazol-4-yl)methoxy)phenyl)acrylic acid (**10k**)*
Yellow solid; Yield:76%;MP = 196–198 ºC; IR (KBr, v$_{max}$) 3285 (NH), 3055 (CH Aromatic), 2940 (CH Aliphatic), 1672 (C=O) Cm^{-1} ^{1}H NMR (499 MHz, DMSO-d6) δ 12.19 (s, 1 H, OH$_{Acid}$), 10.74 (s, 1 H, NH$_{Amide}$), 8.22 (s, 1 H, H Ar), 7.98 (d, $J = 8.2$ Hz, H Ar), 7.76–7.65 (m, 2 H, H Ar), 7.51 (d, $J = 16.0$ Hz, 1 H, H $_{Olefinic}$), 7.40 (t, $J = 7.5$ Hz, 1 H, H Ar), 7.31 (s, 1 H, H Ar), 7.19 (s, 2 H, H Ar), 6.44 (d, $J = 15.9$ Hz, 1 H, H $_{Olefinic}$), 5.44 (s, 2 H, CH$_2$), 5.18 (s, 2 H, CH$_2$), 3.78 (s, 3 H, CH$_{3\ Methoxy}$); ^{13}C NMR (126 MHz, DMSO-d_6) δ 168.32, 165.41, 149.88, 149.60, 144.52, 142.87, 142.75, 134.63, 130.78, 127.95, 126.94, 126.36, 126.01, 125.53, 122.89, 117.38, 113.49, 111.01, 61.93, 55.99, 52.39; ESI-MS (C$_{21}$H$_{19}$N$_5$O$_7$): calculated m/z 453.13 M$^+$, observed m/z 454.06 M$^+$; Anal. Calcd: C$_{21}$H$_{19}$N$_5$O$_7$; C, 55.63; H, 4.22; N, 15.45; Found; C, 55.82; H, 4.43; N, 15.61.

*(E)-3-(3-Methoxy-4-((1-(2-((3-nitrophenyl)amino)-2-oxoethyl)-1H-1,2,3-triazol-4-yl)methoxy)phenyl)acrylic acid (**10 L**)*
Yeloow solid; Yield:79%;MP = 192–193 ºC; IR (KBr, v$_{max}$) 3270 (NH), 3040 (CH Aromatic), 2960 (CH Aliphatic), 1672 (C=O) Cm^{-1}; ^{1}H NMR (499 MHz, DMSO-d_6) δ 12.17 (s, 1H, OH$_{Acid}$), 10.99 (s, 1H, NH$_{Amide}$), 8.58 (s, 1H, H Ar), 8.28 (s, 1H, H Ar), 7.94 (d, $J = 7.8$ Hz, 1H, H Ar), 7.89 (d, $J = 8.3$ Hz, 1H, H Ar), 7.63 (t, $J = 8.2$ Hz, 1H, H Ar), 7.52 (d, $J = 15.9$ Hz, 1H, H $_{Olefinic}$), 7.31 (s, 1H, H Ar), 7.20 (s, 2 H, H Ar), 6.44 (d, $J = 16.0$ Hz, 1H, H $_{Olefinic}$), 5.42 (s, 2 H, CH$_2$), 5.20 (s, 2 H, CH$_2$), 3.79 (s, 3 H, CH$_{3\ Methoxy}$); ^{13}C NMR (126 MHz, DMSO-d_6) δ 168.35, 165.55, 149.88, 149.60, 148.45, 144.46, 142.73, 139.94, 130.88, 127.97, 127.00, 125.68, 122.87, 118.79, 117.46, 113.85, 113.45, 110.99, 61.94, 55.98, 52.67; ESI-MS (C$_{21}$H$_{19}$N$_5$O$_7$): calculated m/z 453.13 M$^+$, observed m/z 454.09 M$^+$; Anal. Calcd: C$_{21}$H$_{19}$N$_5$O$_7$; C, 55.63; H, 4.22; N, 15.45; Found; C, 55.80; H, 4.39; N, 15.63.

*(E)-3-(3-Methoxy-4-((1-(2-((4-nitrophenyl)amino)-2-oxoethyl)-1H-1,2,3-triazol-4-yl)methoxy)phenyl)acrylic acid (**10 m**)*
Yellow solid; Yield:80%; MP = 194–196 ºC; IR (KBr, v$_{max}$) 3260 (NH), 3055 (CH Aromatic), 2945 (CH Aliphatic), 1670 (C=O) Cm^{-1} ^{1}H NMR (499 MHz, DMSO-d_6) δ 12.18 (s, 1 H, OH$_{Acid}$), 11.09 (s, 1 H, NH$_{Amide}$), 8.27 (s, 1 H, H Ar), 8.23 (d, $J = 8.8$ Hz, 2 H, H Ar), 7.82 (d, $J = 8.8$ Hz, 2 H, H Ar), 7.52 (d, $J = 15.9$ Hz, 1 H, H $_{Olefinic}$), 7.31 (s, 1 H, H Ar), 7.19 (s, 2 H, H Ar), 6.44 (d, $J = 15.8$ Hz, 1 H, H $_{Olefinic}$), 5.44 (s, 2 H, CH$_2$), 5.20 (s, 2 H, CH$_2$), 3.78 (s, 3 H, CH$_{3\ Methoxy}$); ^{13}C NMR (126 MHz, DMSO-d_6) δ 168.37, 165.80, 149.86, 149.60, 144.95, 144.42, 143.07, 142.74, 127.98, 126.99, 125.57, 122.86, 119.50, 117.52, 113.47, 111.00, 61.94, 56.01, 52.78; ESI-MS (C$_{21}$H$_{19}$N$_5$O$_7$):

calculated m/z 453.13 M$^+$, observed m/z 454.13 M$^+$; Anal. Calcd: C$_{21}$H$_{19}$N$_5$O$_7$; C, 55.63; H, 4.22; N, 15.45; Found; C, 55.81; H, 4.42; N, 15.66.

(E)-3-(3-Methoxy-4-((1-(2-((2-methyl-4-nitrophenyl)amino)-2-oxoethyl)-1H-1,2,3-triazol-4-yl)methoxy)phenyl) acrylic acid (**10n**)
Brown solid; Yield:67%;MP = 201–203 ºC; IR (KBr, v$_{max}$) 3240 (NH), 3035 (CH Aromatic), 2955 (CH Aliphatic), 1671 (C=O) Cm^{-1} ^{1}H NMR (499 MHz, DMSO-*d$_6$*) δ 12.20 (s, 1 H, OH$_{Acid}$), 10.04 (s, 1 H, NH$_{Amide}$), 8.27 (s, 1 H, H Ar), 8.15 (d, *J* = 1.9 Hz, 1 H, H Ar), 8.06 (d, *J* = 9.6 Hz, 1 H, H Ar), 7.93 (d, *J* = 9.0 Hz, 1 H, H Ar), 7.51 (d, *J* = 15.9 Hz, 1 H, H $_{Olefinic}$), 7.31 (s, 1 H, H Ar), 7.22–7.17 (m, 2 H, H Ar), 6.44 (d, *J* = 16.0 Hz, 1 H, H $_{Olefinic}$), 5.50 (s, 2 H, CH$_2$), 5.19 (s, 2 H, CH$_2$), 3.78 (s, 3 H, CH$_{3\ Methoxy}$), 2.40 (s, 3 H, CH$_{3\ Methyl}$); ^{13}C NMR (126 MHz, DMSO-*d$_6$*) δ 168.31, 165.71, 149.88, 149.83, 143.97, 142.71, 133.66, 130.17, 129.27, 127.94, 127.53, 126.93, 125.62, 122.49, 119.24, 117.38, 113.51, 110.98, 61.94, 56.07, 52.61.; Anal. Calcd: C$_{22}$H$_{21}$N$_5$O$_7$: C, 56.53; H, 4.53; N, 14.98; Found; C, 56.71; H, 4.74; N, 15.14.

(E)-3-(3-Methoxy-4-((1-(2-oxo-2-(phenethylamino)ethyl)-1H-1,2,3-triazol-4-yl)methoxy)phenyl)acrylic acid (**10o**)
Cream solid; Yield:58%;MP = 173–174 ºC; IR (KBr, v$_{max}$) 3190 (NH), 3000 (CH Aromatic), 2920 (CH Aliphatic), 1661 (C=O) Cm^{-1} ^{1}H NMR (499 MHz, DMSO-*d$_6$*) δ 12.17 (s, 1 H, OH$_{Acid}$), 8.43 (t, *J* = 5.5 Hz, 1 H, NH$_{Amide}$), 8.14 (s, 1 H, H Ar), 7.51 (d, *J* = 15.9 Hz, 1 H, H $_{Olefinic}$), 7.32–7.26 (m, 3 H, H Ar), 7.20 (d, *J* = 8.3 Hz, 5 H, H Ar), 6.44 (d, *J* = 15.9 Hz, 1 H, H $_{Olefinic}$), 5.16 (s, 2 H, CH$_2$), 5.07 (s, 2 H, CH$_2$), 3.78 (s, 3 H, CH$_{3\ Methoxy}$), 3.32 (q, *J* = 6.8 Hz, 2 H, CH$_2$), 2.73 (t, *J* = 7.4 Hz, 2 H, CH$_2$); ^{13}C NMR (126 MHz, DMSO-*d$_6$*) δ 168.36, 165.70, 149.89, 149.59, 144.46, 142.54, 139.62, 129.09, 128.82, 127.94, 126.74, 126.63, 122.88, 117.46, 113.44, 110.98, 61.93, 55.98, 52.08, 40.86, 35.36; ESI-MS (C$_{23}$H$_{24}$N$_4$O$_5$): calculated m/z 436.17 M$^+$, observed m/z 437.16 M$^+$; Anal. Calcd: C$_{23}$H$_{24}$N$_4$O$_5$; C, 63.29; H, 5.54; N, 12.84; Found; C, 63.47; H, 5.69; N, 12.98.

AChE and BChE inhibition
Cholinesterase inhibitory activities of all analogs were evaluated spectrometrically using the modified Ellman method as previously reported. 20 μL AChE 0.18 units/mL, or 20 μL BChE iodide 0.162 units/mL and 20 μL DTNB (301 μM) were added to 200 μl sodium phosphate buffer (0.1 mol/L, pH 7.4) in separate wells of a 96-well microplate and gently mixed. Then, 10 μl of different concentrations of test compounds were added to each well and incubated for 15 min at 37 °C followed by the addition of acetylthiocholine (ATCh) or butyrylthiocholine (BTCh) (20 μl, final concentration of 452 μM) to produce the yellow anion of 5-thio-2-nitrobenzoic acid. The absorbance of each well was measured at 415 nm using a microplate reader. IC$_{50}$ and inhibition values were calculated with the software GraphPad Prism as the mean of three independent experiments and expressed as mean ± SEM[47].

Enzyme kinetic studies against BChE
As previously reported, the kinetic study of BChE was carried out at five different concentrations of compound **10j** and butyrylthiocholine substrate (0.1–1 mM) by Ellman's method[48].

Tyrosinase inhibitory activity
Tyrosinase inhibitory activity was determined based on the procedure previously described, with a slight modification. In brief, the test reaction mixture comprised 10 μL of each derivative, and 10 μL of mushroom tyrosinase (500 units; Sigma-Aldrich, St Louis, MO, USA) in 160 potassium phosphate buffer (pH = 6.8). The reaction mixture was incubated at 37 °C for 20 min and then 20 μL of L-Dopa (0.5 mmol/L) was added to each well, and the absorption was measured at 475 nm. The absorbance of the same mixture without tyrosinase was used as the control. Kojic acid was used as a positive control. The optical density of the inhibition in the control was considered to represent 100%. The data are expressed as mean percentages and the results were repeated in triplicate[49,50].

Molecular docking
The molecular docking approach was performed using induced-fit molecular docking (IFD) of the Schrodinger package. The Maestro software package's SMILE format of **10j** was converted to a three-dimensional structure. The X-ray structures of BChE (PDB code: 4BDS) were prepared with the Protein Preparation Wizard interface of Maestro *via* removing the ligand and water molecules, adding hydrogen atoms, optimizing their position, and assigning the ionization states of acid and basic residues according to PROPKA prediction at pH 7.0. The molecular docking was performed using IFD mode with the ligands as flexible, the force field was set as OPLS-2005, and all other parameters were set to default. The binding site was used to generate the grid for IFD calculation. The maximum 20 poses with receptor and ligand van der Waals radii of 0.7 and 0.5, respectively considered. Residues within 8 Å of the crystallographic ligands at the active site were refined, followed by side-chain optimization. Structures in which prime energy is more than 30 kcal/mol are eliminated. The re-docking experiment for validation of the used docking protocol was done and recorded the RMSD value of 0.79, indicating the docking experiment is reliable.

Molecular dynamics simulation
Molecular dynamics simulations were conducted following the procedures previously reported[51].

DFT method

DFT calculations were conducted for compound **10j** as the most active compound using Gaussian version 09 (https://gaussian.com/glossary/g09/)[52]. The results were visualized using GaussView version 6.0 (https://gaussian.com/gaussview6/). The compounds under consideration were optimized using the B3LYP/6-31G (d, p) level basis set without any symmetrical constraints. The frontier molecular orbitals (HOMO and LUMO) and ESP were obtained from the optimized geometry.

Data availability

The datasets generated and/or analyzed during the current study are available in the Worldwide ProteinData Bank with PDB ID of 4BDS repository.

References

1. Safaeian, L., Asghari-Varzaneh, M., Alavi, S-S., Halvaei-Varnousfaderani, M. & Laher, I. Cardiovascular protective effects of cinnamic acid as a natural phenolic acid: A review. *Arch. Physiol. Biochem.* 1–11 (2024).
2. Jacob, B., Baba, H., Oluwadiya, J. & Synthesis Characterization and evaluation of Anti-inflammatory and antimicrobial properties of some cinnamic acid derivatives. *Nigerian J. Pharmac Res.* **16**(1), 1–8 (2020).
3. Deng, H. et al. Application of cinnamic acid in the structural modification of natural products: A review. *Phytochemistry* **206**, 113532 (2023).
4. Rasool, A. et al. Bis-pharmacophore of cinnamaldehyde-clubbed thiosemicarbazones as potent carbonic anhydrase-II inhibitors. *Sci. Rep.* **12**(1), 16095 (2022).
5. Islam, M. et al. Synthesis and biological evaluation of 2-nitrocinnamaldehyde derived thiosemicarbazones as urease inhibitors. *J. Mol. Struct.* **1284**, 135387 (2023).
6. Ruwizhi, N. & Aderibigbe, B. A. Cinnamic acid derivatives and their biological efficacy. *Int. J. Mol. Sci.* **21**(16), 5712 (2020).
7. Falbo, F. et al. Synthetic derivatives of natural cinnamic acids as potential anti-colorectal cancer agents. *Chem. Biol. Drug Des.* **103**(1), e14415 (2024).
8. Mingoia, M. et al. Synthesis and biological evaluation of novel cinnamic acid-based antimicrobials. *Pharmaceuticals* **15**(2), 228 (2022).
9. Bargagna, B. et al. Multifunctional Small molecules as potential anti-Alzheimer's disease agents. *Molecules* **26**(19), 6015 (2021).
10. Fernandez-Bolanos, J. G. & Lopez, O. Butyrylcholinesterase inhibitors as potential anti-Alzheimer's agents: An updated patent review (2018-present). *Exp. Opin. Ther. Pat.* **32**(8), 913–932 (2022).
11. Romagnoli, R. et al. Cinnamic acid derivatives linked to arylpiperazines as novel potent inhibitors of tyrosinase activity and melanin synthesis. *Eur. J. Med. Chem.* **231**, 114147 (2022).
12. Fernandes, B., Cavaco-Paulo, A. & Matamá, T. A comprehensive review of mammalian pigmentation: Paving the way for innovative hair colour-changing cosmetics. *Biology* **12**(2), 290 (2023).
13. Li, C., Kuai, L., Cui, R. & Miao, X. Melanogenesis and the targeted therapy of melanoma. *Biomolecules* **12**(12), 1874 (2022).
14. Snyman, M., Walsdorf, R. E., Wix, S. N. & Gill, J. G. The metabolism of melanin synthesis—From melanocytes to melanoma. *Pigment Cell. Melanoma Res.* (2024).
15. Sheng, Z. et al. Design, synthesis and evaluation of cinnamic acid ester derivatives as mushroom tyrosinase inhibitors. *MedChemComm* **9**(5), 853–861 (2018).
16. Lin, Z., Xia, W., Liu, R., Jiang, S. & Ma, Z. Synthesis of cinnamic acid-coumarin ester analogs and inhibition of tyrosinase activity. *Chin. J. Organ. Chem.* **40**(9), 2980 (2020).
17. Tang, K. et al. Design, synthesis of Cinnamyl-paeonol derivatives with 1, 3-Dioxypropyl as link arm and screening of tyrosinase inhibition activity in vitro. *Bioorgan Chem.* **106**, 104512 (2021).
18. Ahmadi, F. et al. Efficient synergistic combination effect of curcumin with piperine by polymeric magnetic nanoparticles for breast cancer treatment. *J. Drug Deliv Sci. Technol.* **86**, 104624 (2023).
19. Iraji, A., Khoshneviszadeh, M., Firuzi, O., Khoshneviszadeh, M. & Edraki, N. Novel small molecule therapeutic agents for Alzheimer disease: Focusing on BACE1 and multi-target directed ligands. *Bioorgan Chem.* **97**, 103649 (2020).
20. Oliyaei, N., Moosavi-Nasab, M., Tanideh, N. & Iraji, A. Multiple roles of fucoxanthin and astaxanthin against Alzheimer's disease: Their pharmacological potential and therapeutic insights. *Brain Res. Bullet.* **193**, 11–21 (2023).
21. Karimi, A. H. et al. Design and synthesis of multi-target directed 1, 2, 3-triazole-dimethylaminoacryloyl-chromenone derivatives with potential use in Alzheimer's disease. *BMC Chem.* ;**14**(1). (2020).
22. Tokalı, F. S., Taslimi, P., Usanmaz, H., Karaman, M. & Şendil, K. Synthesis, characterization, biological activity and molecular docking studies of novel schiff bases derived from thiosemicarbazide: Biochemical and computational approach. *J. Mol. Struct.* **1231**, 129666 (2021).
23. Tokalı, F. S. et al. Design, synthesis, molecular docking, and some metabolic enzyme inhibition properties of novel quinazolinone derivatives. *Arch. Pharm.* **354**(5), 2000455 (2021).
24. Tokalı, F. S. et al. Novel quinazolinone derivatives: Potential synthetic analogs for the treatment of glaucoma, Alzheimer's disease and diabetes mellitus. *Chem. Biodiv*. **20**(10), e202301134 (2023).
25. Tokalı, F. S., Sağlamtaş, R., Öztekin, A., Yırtıcı, Ü. & Çomaklı, V. New Diacetic acids containing quinazolin-4(3H)-one: Synthesis, characterization, anticholinergic properties, DFT analysis and molecular docking studies. *ChemistrySelect* **8**(10), e202205039 (2023).
26. Tokalı, F. S., Alım, Z. & Yırtıcı, Ü. Carboxylate- and sulfonate-containing quinazolin-4(3H)-one rings: Synthesis, characterization, and carbonic anhydrase I–II and acetylcholinesterase inhibition properties. *ChemistrySelect* **8**(8), e202204191 (2023).
27. Tokalı, F. S. et al. Synthesis of new carboxylates and sulfonates containing thiazolidin-4-one ring and evaluation of inhibitory properties against some metabolic enzymes. *J. Iran. Chem. Soc.* **20**(10), 2631–2642 (2023).
28. Gießel, J. M., Serbian, I., Loesche, A. & Csuk, R. Substituted cinnamic anhydrides act as selective inhibitors of acetylcholinesterase. *Bioorgan Chem.* **90**, 103058 (2019).
29. Ghafary, S. et al. Novel cinnamic acid–tryptamine hybrids as potent butyrylcholinesterase inhibitors: Synthesis, biological evaluation, and docking study. *Arch. Pharm.* **351**(10), 1800115 (2018).
30. Ghafary, S. et al. Design, synthesis, and evaluation of novel cinnamic acid-tryptamine hybrid for inhibition of acetylcholinesterase and butyrylcholinesterase. *DARU J. Pharmac Sci.* **28**(2), 463–477 (2020).
31. Sepehri, N. et al. Synthesis, characterization, molecular docking, and biological activities of coumarin–1,2,3-triazole-acetamide hybrid derivatives. *Arch. Pharm.* **353**(10), 2000109 (2020).
32. Hosseini, S., Pourmousavi, S. A., Mahdavi, M. & Taslimi, P. Synthesis, and in vitro biological evaluations of novel naphthoquinone conjugated to aryl triazole acetamide derivatives as potential anti-Alzheimer agents. *J. Mol. Struct.* **1255**, 132229 (2022).

33. Bhagat, K. et al. Novel series of triazole containing coumarin and isatin based hybrid molecules as acetylcholinesterase inhibitors. *J. Mol. Struct.* **1245**, 131085 (2021).
34. Khan, S. A., Akhtar, M. J., Gogoi, U., Meenakshi, D. U. & Das, A. An overview of 1,2,3-triazole-containing hybrids and their potential anticholinesterase activities. *Pharmaceuticals* ;**16**(2). (2023).
35. Enkhtaivan, E. & Lee, C. H. Role of Amine neurotransmitters and their receptors in skin pigmentation: therapeutic implication. *Int. J. Mol. Sci.* **22**(15). (2021).
36. Jin, W., Stehbens, S. J., Barnard, R. T., Blaskovich, M. A. T. & Ziora, Z. M. Dysregulation of tyrosinase activity: A potential link between skin disorders and neurodegeneration. *J. Pharm. Pharmacol.* **76**(1), 13–22 (2024).
37. Tan, A. & Almaz, Z. A series of 1, 2, 3-triazole compounds: Synthesis, characterization, and investigation of the cholinesterase inhibitory properties via in vitro and in silico studies. *J. Mol. Struct.* **1277**, 134854 (2023).
38. Askarani, H. K. et al. Design and development of multi-target directed 1, 2, 3-triazole-dimethylaminoacryloyl-chromenone derivatives with potential use in Alzheimer's disease. (2020).
39. Nazir, Y. et al. Hydroxyl substituted benzoic acid/cinnamic acid derivatives: Tyrosinase inhibitory kinetics, anti-melanogenic activity and molecular docking studies. *Bioorgan Med. Chem. Lett.* **30**(1), 126722 (2020).
40. Garcia-Jimenez, A. et al. Catalysis and inhibition of tyrosinase in the presence of cinnamic acid and some of its derivatives. *Int. J. Biol. Macromol.* **119**, 548–554 (2018).
41. Ullah, S. et al. Tyrosinase inhibition and anti-melanin generation effect of cinnamamide analogues. *Bioorgan Chem.* **87**, 43–55 (2019).
42. Takahashi, T. & Miyazawa, M. Tyrosinase inhibitory activities of cinnamic acid analogues. *Die Pharm. Int. J. Pharmac Sci.* **65**(12), 913–918 (2010).
43. Kishore, D. R., Mounika, K., Goel, K., Naveen, J. & Satyanarayana, G. Microwave-assisted domino povarov-type [4 + 2] cycloaddition: A rapid access to 7-phenyl-6H-chromeno [4, 3-b] quinolines. *Synthesis* **55**(05), 808–820 (2023).
44. Mahdavi, M. et al. Synthesis of new benzimidazole-1, 2, 3-triazole hybrids as tyrosinase inhibitors. *Chem. Biodiv.* **15**(7), e1800120 (2018).
45. Ansari, S. et al. Design, synthesis, and α-glucosidase-inhibitory activity of phenoxy-biscoumarin–N-phenylacetamide hybrids. *Arch. Pharm.* **354**(12), 2100179 (2021).
46. Li, L., Chen, M. & Jiang, F-C. Design, synthesis, and evaluation of 2-piperidone derivatives for the inhibition of β-amyloid aggregation and inflammation mediated neurotoxicity. *Bioorgan Med. Chem.* **24**(8), 1853–1865 (2016).
47. Nazarian, A. et al. Anticholinesterase activities of novel isoindolin-1,3-dione-based acetohydrazide derivatives: Design, synthesis, biological evaluation, molecular dynamic study. *BMC Chem.* **18**(1), 64 (2024).
48. Pourtaher, H., Hasaninejad, A., Zare, S., Tanideh, N. & Iraji, A. The anti-Alzheimer potential of novel spiroindolin-1,2-diazepine derivatives as targeted cholinesterase inhibitors with modified substituents. *Sci. Rep.* **13**(1), 11952 (2023).
49. Bagheri, A., Moradi, S., Iraji, A. & Mahdavi, M. Structure-based development of 3,5-dihydroxybenzoyl-hydrazineylidene as tyrosinase inhibitor: In vitro and in silico study. *Sci. Rep.* **14**(1), 1540 (2024).
50. Noori, M. et al. Phenyl-quinoline derivatives as lead structure of cholinesterase inhibitors with potency to reduce the GSK-3β level targeting Alzheimer's disease. *Int. J. Biol. Macromol.* **253**(Pt 7), 127392 (2023).
51. Pourtaher, H., Mohammadi, Y., Hasaninejad, A. & Iraji, A. Highly efficient, catalyst-free, one-pot sequential four-component synthesis of novel spiroindolinone-pyrazole scaffolds as anti-Alzheimer agents: in silico study and biological screening. *RSC Med. Chem.* **15**(1), 207–222 (2024).
52. Gaussian 09, Revision, A. et al. J. W. K. Morokuma, O. Farkas, J. B. Foresman, and D. J. Fox, Gaussian, Inc., Wallingford CT, 2016.

Author contributions

A.S.S.A, M.H.S, A.H.A, S.N.G, M.N, N.D. synthesized compounds and contributed to the characterization of compounds. M.H.H, C.I and B.L. performed biological. M.A and J.M in silico study. A.I and M.M supervised the study. All authors read and approved the final version of the article.

Funding

Declarations

Competing interests

The authors declare no competing interests.

Additional information

Supplementary Information The online version contains supplementary material available at https://doi.org/10.1038/s41598-024-83020-3.

Correspondence and requests for materials should be addressed to M.M. or A.I.

Reprints and permissions information is available at www.nature.com/reprints.

Publisher's note Springer Nature remains neutral with regard to jurisdictional claims in published maps and institutional affiliations.